Kinetics of Low Field Gradient Magnetophoresis in the Presence of Magnetically Induced Convection

Sim Siong Leong[†], *Zainal Ahmad*[†], *Juan Camacho*[§], *Jordi Faraudo*[§§], *JitKang Lim*[*,†,‡]

[†]School of Chemical Engineering, Universiti Sains Malaysia, Nibong Tebal, Penang 14300, Malaysia.

[§]Departament de Física, Facultat de Ciències, Universitat Autònoma de Barcelona, E-08193 Bellaterra, Spain

[§§]Institut de Ciència de Materials de Barcelona (ICMAB-CSIC), C/ dels Til.lers s/n, Campus UAB, E-08193 Bellaterra, Spain.

[‡]Department of Physics, Carnegie Mellon University, Pittsburgh, PA 15213, USA.

*****To whom correspondence should be addressed:

JitKang Lim

School of Chemical Engineering

Engineering Campus,

Universiti Sains Malaysia, Seri Ampangan,

14300 Nibong Tebal, Penang, Malaysia.

e-mail: chjitkangl@usm.my

tel: +60-4-599-6423

fax: +60-4-599-1013

Abstract

Previous work (Leong et al., Soft Matter 2015,11, 6968) has demonstrated, by using both experiments and simulations, that magnetic field gradient can induce substantial convective currents during magnetophoresis of superparamagnetic nanoparticles in the solution. This effect substantially enhances the efficiency of low gradient magnetic separation (LGMS) processes. Throughout the LGMS process, this circulating flow plays a dominant role in homogenizing the nanoparticle solution and enhancing the vertical motion of particles. Here we perform a detailed quantitative study of the factors affecting the kinetics of LGMS in the presence of magnetically induced convection. In particular, we have found that the magnetophoretic collection rate of magnetic nanoparticles in LGMS is solely determined by the magnetic field gradient at the surface of contact of the dispersion cuvette with the magnet (denoted as “particles collection plane” in this work) and the area of this surface. Surprisingly, the kinetics of LGMS is independent of the magnetic field distribution across the solution subjected to magnetophoresis as long as magnetically induced convection presents. These conclusions are of crucial relevance in the design of low gradient magnetic separator for engineering applications.

1. Introduction

The ability to control the motion of nanoparticles under an external force field, which subsequently leads to their separation from the surrounding media, is of both fundamental and practical importance. Concurrently, many techniques have been developed to achieve this target, including electrophoresis,[1] dielectrophoresis,[2] electroomosis,[3] magnetophoresis,[4] optical tweezer[5] and etc. Out of all the technique developed, magnetic separation has several advantages over other methods, especially for bio-related applications, due to its non-invasive nature,[6] easy to be miniaturized,[7] well defined magnetic force field[7] and a wide selection of magnetic nanoparticles are available for tagging purpose.[8] In practice, the separation of magnetic particles has demonstrated its feasibility in plenty of applications such as drug delivery,[9-11] microassembly[12, 13] and nanoscale separation.[14, 15] Additionally, magnetic separation is playing a predominant role in biomedical cell separation, particularly in the separation of *Salmonella enterica* (by antibody conjugated magnetic nanoparticles),[16] mouse macrophages and human ovarian cancer (HeLa) cells (by internalization of magnetic particles into the cells),[17] biotinylated substrate (by streptavidin magnetic particles)[18] as well as leukemia cells and prostate cancer cells (by fluorescent-magnetic-biotargeting multifunctional nanobioprobes).[19]

The process in which the magnetic particles move in relative to their surrounding fluid, in response to an externally applied magnetic field, is known as magnetophoresis.[20] In fact, this process has found many uses in mineral processing and mining industry.[21] Up-to-date, all the conventional technologies working on magnetophoresis driven separation, which has been widely implemented for engineering applications, are mostly operated in separation columns characterized by high magnetic field gradients (this process is known as high gradient magnetic separation, HGMS).[22, 23] Theoretical calculations (by using typical values for fluid flow and geometry, viscosity, and magnetic properties) show that magnetic field gradient of the order of

10^4 T/m – 10^5 T/m are needed for fast removal and efficient capture of the dispersed magnetic particles. In HGMS processes, magnetic field gradient is typically generated by the distortion of magnetic field (usually imposed by electromagnet) by the magnetizable packing materials which fill the packed bed column. The magnetic field gradient generated in this way is extremely intense and highly localized, which presents only near the steel wool fibers where particles become trapped. However, in many applications of magnetic nanoparticles (MNPs) in solution, such as biomedical applications, this strategy is not appropriate. The preferred strategy in these cases is the employment of permanent magnet(s)[23-25], which are located outside the particles suspension, for a distal control of the particles motion in a non-contact mode. This strategy is known as low gradient magnetic separation (LGMS), which has been widely utilized by chemical engineers and chemist to recollect the magnetic responsive material in the removal of contaminants such as dye,[26] heavy metal ions,[27] toxic organic compound[28] as well as microalgae[29] in laboratory scale. Nonetheless, the implementation of LGMS in real-time application is technically challenging as MNPs experience much lower magnetic field gradient ($\nabla B < 100\ \mathrm{T/m}$) which renders the rapid isolation of MNPs beyond the bound of possibility. Therefore, new strategies (the design of both geometry configuration of the magnetic separator as well as MNPs) are needed in order to bring LGMS into the realm of practicability.[24, 25, 30-33] Strategies for LGMS should be able to employ new physical effects, which are relevant to the magnetophoresis of MNPs under low magnetic field gradient, to enhance the low magnetophoretic separation rate that is expected theoretically. Recent works propose two different kinds of effects which are able to enhance the magnetophoretic separation rate of LGMS: magnetic cooperative effect[31] and hydrodynamic effect.[34] While the first effect has been discussed in the literature in the previous years (see reviews in Ref[35-37]), the second one was proposed in a recent paper for the first time.[34]

Magnetic cooperative effects proposed in Ref[31] are based on the fact that, for strong enough interparticle magnetic interactions and for large enough particle concentrations (technically for aggregation numbers N* larger than 1),[11, 36, 37] superparamagnetic particles tend to form elongated clusters which are able to move more rapidly than individual particles under a magnetic field gradient. This phenomenon is further supported by computation simulation of the dynamical behavior of MNPs under an externally applied magnetic field. For instance, by performing simulation based on Brownian dynamics,[38] Langevin dynamics[39] and *on-the-fly* coarse grain model,[40] MNPs aggregates were formed under magnetic field. In Ref[31], magnetophoretic velocities as large as several centimeter per minute were observed for concentrated dispersions (~10 g/L) of superparamagnetic colloidal particles (with diameters of 200 nm and 400 nm) under magnetic field gradient of 30 T/m – 60 T/m. In this case, the observed magnetophoretic velocity decays with the reduction in particles concentration[31] (due to the formation of smaller size self-assembled chains of particles as concentration decreases). At very low particle concentration, for the case in which interparticle magnetic interaction and chain formation are insignificant, the magnetophoretic velocity of particle diminishes to the low value predicted by the conventional magnetophoresis model.[36, 41, 42] It is important to recall here that these works considered a quiescent fluid under a nearly uniform magnetic gradient, in order to have equivalent magnetophoretic conditions across all the system (see Figure 1a).

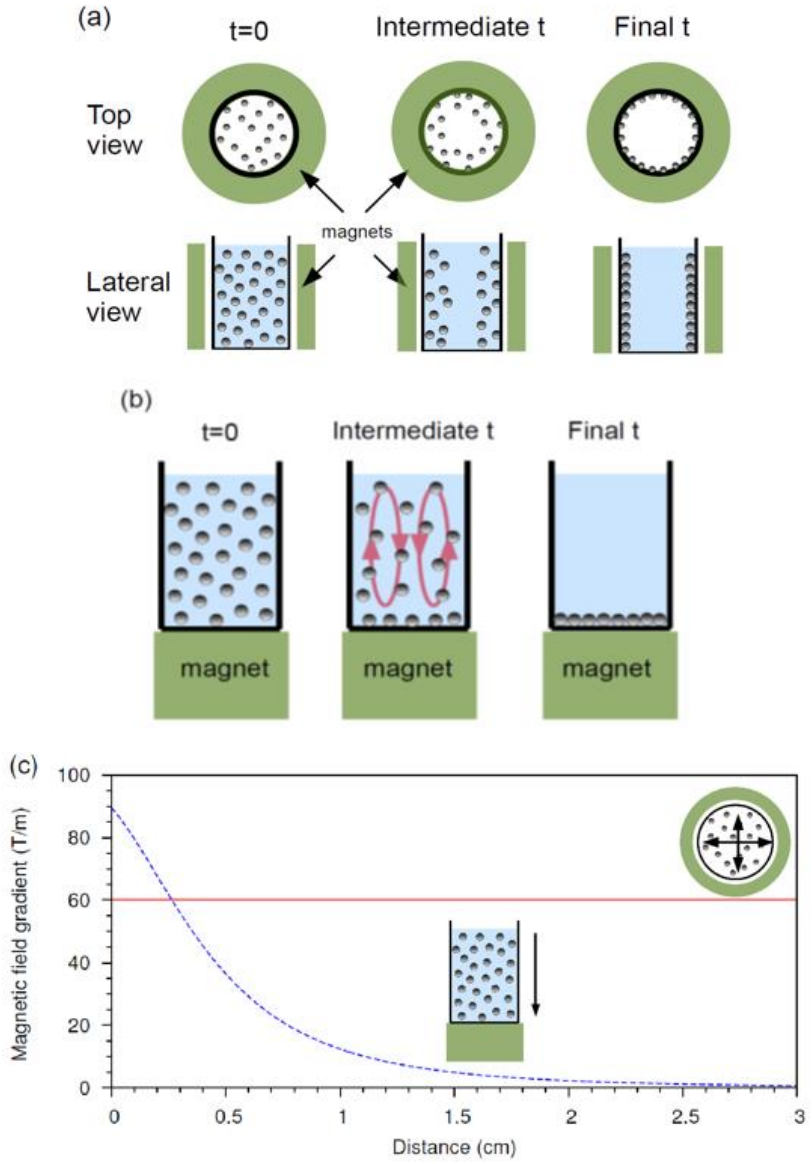

Figure 1. *Scheme with different low gradient magnetic separation (LGMS) of magnetic nanoparticles (MNPs) in solution, indicating the arrangement of magnets (in green) and the location of the particles at different stages of the separation process. (a) LGMS in a homogeneous magnetic gradient, generated by a cylindrical arrangement of magnets around a bottle or vial containing the solution. (b) LGMS in an inhomogeneous magnetic field gradient induced by a hand magnet (the red arrows indicate spontaneous motion of fluid) (c) Comparison of typical magnetic field gradients employed in the setups depicted in (a) and (b). For homogeneous LGMS, the maximum employed gradient in experiments is ~60 T/m. For*

inhomogeneous LGMS, the magnetic field gradient profile was calculated from Equation (8) in Ref[34] using the data for a typical magnet (grade N50 NdFeB cylindrical magnet, height 1.5 cm, radius 0.7 cm and remanent magnetization 1.5 T).

A different approach[34] considers the use of non-uniform magnetic gradients, by simply placing a permanent magnet below the cuvette containing the dispersion, as shown in Figure 1b. From the perspective of established theory, this set-up may seem inefficient, since the magnetic field gradient (responsible for magnetophoretic motion) is only significant near the bottom of the cuvette and decay tremendously with the displacement from the magnet (see Figure 1c). However, as shown dramatically for the first time in our previous work,[34] a new hydrodynamic effect appears for this inhomogeneous field gradient configuration (Figure 1b) which is not observed in the homogeneous field gradient situation (Figure 1a). In the experiments reported in our previous work,[34] the huge difference in magnetic field gradient (and consequently, in magnetophoretic velocities) between the bottom and the top of the system imparts the much higher magnetophoretic velocity to the MNPs located at the bottom in comparison to those located at the upper part of the solution. Such a situation leads to the more rapid clearance of the MNPs at the bottom and gives rise to a vertical concentration gradient (concentration of MNPs is lowest at the bottom of the cuvette and increases with elevation) which renders the system to become mechanically unstable. In this regard, convective motion of the fluid is developed to homogenize the system and eliminate the mechanical instability of the system, as shown in Figure 1b. Such a situation is not observed under a homogeneous magnetic field gradient due to the absence of the MNPs concentration gradient, which leads to the mechanical instability of the solution system (even though the momentum transfer between the particle-and-fluid still happening), throughout the process. For the particular example considered in our previous work,[34] (magnetophoresis of 30 nm iron oxide MNPs under a

permanent magnet), both experimental and simulation data show that the magnetically induced convection boosts the magnetophoretic separation rates, being about 30 times faster as compared with the situation with no convection. Interestingly, in these experiments, particles move independently (without forming chains or aggregates) since their mutual magnetic interaction is too weak and all the increase in separation rates is due to the hydrodynamic effect (the convective motion).

It is clear that in order to optimize the magnetophoretic collection of MNPs in a magnetic separator and decide between the different options in the design of LGMS (such as concentration of MNPs dispersion, homogeneous or inhomogeneous magnetic field gradient, geometrical arrangement of magnetic sources, etc.), it is crucial to understand the underlying mechanisms of the process and identify the factors that exert significant impact on the MNPs separation rate. Our previous work[34] clearly demonstrates the need for a deeper understanding of these factors, particularly the role of hydrodynamic effect. Our purpose in this work is to study in detail the kinetics of magnetophoresis in the presence of magnetically induced convection (the situation in Figure 1b), quantifying the impact of the different variables in magnetophoresis separation rate (effects of the magnetic field distribution, volume of the MNPs suspension, and size of MNPs). The experimental results will be compared with a simple mathematical model which offers a minimalistic yet accurate description of the magnetophoresis kinetics. The proposed picture of low gradient magnetophoresis might serve as the golden rule of thumb in designing a magnetic separator with improved efficiency.

This work emphasizes on the dynamical behavior of LGMS which is conducted in batchwise manner as depicted in Figure 1b. However, it should be noted that the isolation of magnetic particles by low gradient magnetic field can also be performed in continuous magnetic separator. For instance, Xia and coworkers show that magnetic particles tagged *E. coli*) were deviated from its original migration pathway and eventually being separated by a

low gradient magnetic separator.[43] In addition, Pamme and coworkers demonstrated the successful separation of cell loaded with MNPs in microfluidic magnetic separation device operated in continuous manner.[17] The magnetophoretic isolation of magnetic micro/nano-particles from solution that is flowing through microfluidic magnetic separator is also predicted by analytical models developed by Furlani and coworkers (this models take particle-fluid interaction into consideration).[44-46] Continuous magnetic separator is particular advantageous for its high throughput and ease of operation. Nevertheless, batchwise magnetic separation process has also being widely employed in bio-related or waste removal applications due to its less intricate magnetic separation device and lower equipment cost. Furthermore, batchwise magnetic separation process is relatively simple, in comparison to continuous process, for us to conduct mathematical analysis on the kinetic of LGMS leading to better understanding on the working principle of this process. Once the fundamental mechanism of batchwise LGMS process is revealed, the same principle can be generalized to continuous LGMS process which is more complicated and characterized by occurrence of force convective flow.

2. Modeling the kinetics of magnetophoresis in the presence of magnetic convection

2.1 Limitations of the classical picture

Before formulating the new model discussed in this paper, it is useful to discuss the conventional magnetophoresis model and its limitations at the first place. Consider the situation shown in Figures 1a and b, assuming that the interparticle magnetic interaction is insignificant and can be neglected as in the experiments in previous publications.[34, 41, 47] This is a reasonable assumption as the non-interacting nature of our particle system has been reported by our previous work in which the aggregation parameter is less than unity in the bulk solution.[34] The

n-component magnetophoretic force experienced by a magnetic particle in the solution $F_{m,z}$ is given by (the detailed derivation of Equation (1) is given in Appendix A1):

$$F_{m,z} = m\frac{\partial B}{\partial z} = \frac{\pi d^3 M}{6}\frac{\partial B}{\partial z} \tag{1}$$

where m is the magnetic dipole of the particle, M its magnetization per unit volume, d is the diameter of the magnetic core of the particle and B is the modulus of the (external) magnetic field strength. In the case shown in Figure 1a, the magnetic field gradient and the magnetophoretic force are directed in the radial direction (towards the separator walls) whereas the magnetic field gradient and magnetophoretic force is parallel to the z-direction (pointing towards the magnet) in the case of Figure 1b. In the absence of other forces, the magnetophoretic velocity of a particle can be obtained by equating the magnetophoretic force given by Equation (1) and the viscous drag F_D experienced by a particle moving with velocity v (relative to the surrounding fluid), which is given by the Stokes equation:

$$F_D = 3\pi\eta d_H v \ , \tag{2}$$

where d_H is the hydrodynamic diameter and η is the viscosity of the suspension. By equating Equations (1) and (2), the expression of the magnetophoretic velocity v_m of a MNP is obtained as below:[31, 35]

$$v_m = \frac{d^3 M}{18 d_H \eta}\frac{\partial B}{\partial z} \ . \tag{3}$$

This model has successfully described real time LGMS with uniform magnetic field gradient[41, 42, 47] which has accurately predicted the magnetophoretic separation times performed with a setup as in Figure 1a by using diluted systems with negligible interparticle magnetic interaction. As shown by experiments, simulations and analytical theory, the separation process in this case proceeds as shown schematically in Figure 1a. Particles move in the radial direction towards

the walls of the system and a clear region (without particles) is created in the center of the system, whose particle front (the boundary which separates region with and without particles) is advancing towards the walls. However, Equation (3) fails to predict magnetophoretic separation time with the setup shown in Figure 1b, which corresponds to an inhomogeneous magnetic field gradient.[34] In a LGMS with a single magnet as shown in Figure 1b, Equation (3) implies that the magnetophoretic velocity of the particles will decrease with the displacement from the magnet z, since the magnetic field strength and the magnetic field gradient decrease as z increases, as shown in Figure 1c. This condition implies that, as time passes, an initially homogeneous distribution of particles will become inhomogeneous, with higher concentration on the top of the system and lower concentration at the bottom. Previous computer simulations of magnetophoresis models in which hydrodynamic effects are ignored also predicted the generation of an inhomogeneous concentration profile under an inhomogeneous magnetic field gradient.[34, 42] This prediction of the model is not in agreement with the experiments reported in our previous work,[34] in which a homogeneous concentration is observed throughout the entire timescale of the experiment. The evolution of the separation process in our previous work[34] proceeds as shown schematically in Figure 1b. After placing an initially homogeneous dispersion over the magnet, convective currents (not considered in Equation (3)) are observed to appear in the fluid. The concentration of particles is observed to decrease with time homogeneously within the whole dispersion and the particles accumulate at the bottom of the cuvette. It is also important to recall that the kinetics of the process is faster than expected from Equation (3).

Since magnetic force experienced by MNPs is directly proportional to magnetic field gradient (Equation (1)), MNPs located further away from magnet experience significant shortfall in magnetic pulling, and the model predicts extraordinarily slow and ineffective magnetophoretic separation. For example, consider the magnetic field gradient generated by

grade N50 neodymium ferrite boron (NdFeB) permanent cylindrical magnet (as shown in Figure 1c) decays from ~90 T/m to 0.84 T/m as one departs from the bottom of the cuvette to 3 cm of elevation along its axis, featuring a rapid decline of magnetic field gradient over 100 times with respect to the displacement. From our calculation, a 30 nm MNPs is experiencing magnetophoretic force of 7.02×10^{-19} N which translated to magnetophoretic velocity of 2.78 nm/s (Figure 2a). At this velocity, the particle requires approximately 20 days (Figure 2b) to travel a short distance of 3 cm to the magnetic source and being separated (Please refer to Supporting Information S1 for details of this calculation). In the absence of other transport mechanisms, this calculation directly rejects the possibility of using a single magnet as in Figure 1b for manipulating the motion of MNPs which subsequently leads to their separation. However, the experiments in Ref[34] for this system show an exponential decrease of the number of particles in solution with a decay time of ~11 h, much faster than the predictions of this simple model.

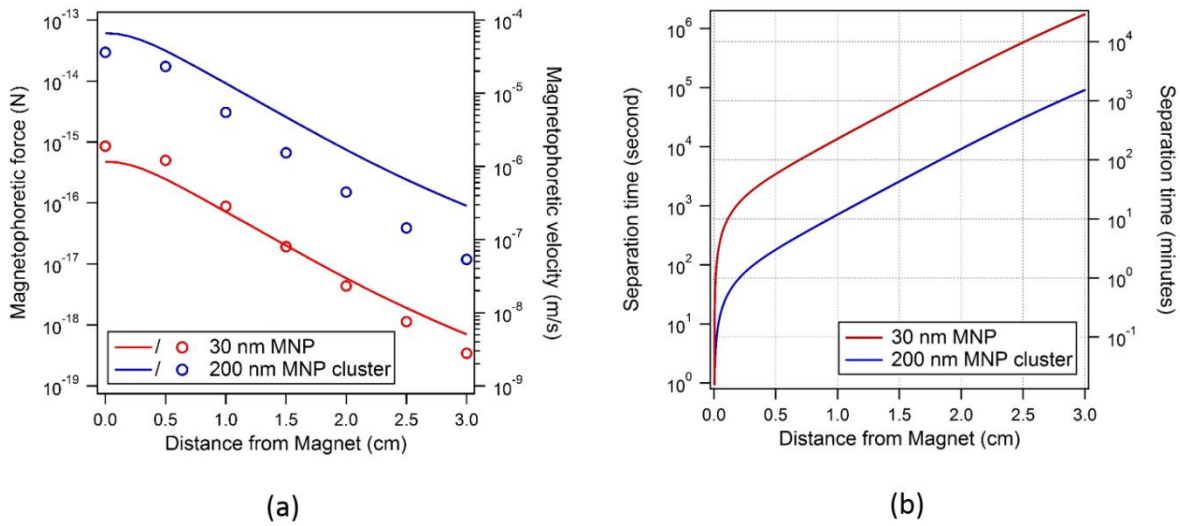

Figure 2. *(a) Magnetophoretic force (solid line) and magnetophoretic velocity (circular dots) experienced by 30 nm MNPs and 200 nm MNPs cluster with respect to distance from magnet. The calculation was performed by using grade N50 NdFeB cylindrical permanent magnet which height and radius at 1.5 cm and 0.7 cm respectively. The magnet is axially magnetized*

with remanent magnetization of 1.45 T. (b) The plot of separation time of MNPs versus their displacement from the magnet pole. Here, the separation time is defined as the time required for the particular MNP to travel from the given displacement to the magnet pole and being segregated.

We expect these convective effects to be present in the experimental setup of Figure 1b not only for dispersions of small NPs but also for larger particles, for example for particles consisting of clusters of MNPs. For instance, the predictions of Equations (1) and (2) for the magnetophoretic force and magnetophoretic velocity attained by a 200 nm MNPs cluster at distance 3 cm away from the magnet are given by 8.95×10^{-17} N and 53.3 nm/s respectively (Figure 2a), which are much larger compared to that of a single 30 nm MNP. Nonetheless, about 25 hours are still required for the given MNPs cluster to be captured and separated out from the solution (Figure 2b). In fact, such calculation of MNPs cluster separation time has been overestimated due to the following reasons: (1) saturation magnetization of MNPs (~70 emu/g)[48] was assumed throughout the calculation (in reality, MNPs possess lower magnetization in region with lower magnetic field strength and hence would experience lower magnetophoretic force) and (2) the most densely arranged sphere packing (face-centered cubic) was adopted in the calculation of magnetic material volume in a MNPs aggregate which packing factor is given by 0.74.[49] Despite of that, for 200 nm MNPs aggregate which is as close as 1.5 cm away from the magnet, the separation time is theoretically calculated as 43 minutes (Figure 2b). This separation time is still almost 3 times longer in comparison to that of experimental observation, which only requires 15 minutes to achieve complete separation (Table 1, Row 4). Moreover, the experimental examples compiled in Table 1 for experiments employing the setup shown in Figure 1b, show that the separation time predicted by force balance (Equation (2)) is always greater than the experimentally observed separation time for

LGMS. We expect that the magnetically induced convective effect illustrated in Figure 1b is present in all these experimental conditions. In principle, computer simulations including a full hydrodynamic description (as the ones performed in Ref[34]) can be done for predictions in every experimental situation. However, these simulations are computationally demanding and complex. In practice, it will be far more useful to be able to obtain a simple analytical equation, extending the classical model given by Equation (1) – (3) to include –at least approximately- the convective effect which is now missing in the model. This is precisely the purpose of the next subsection.

Table 1. *Results for LGMS of nanoparticle using the setup shown in Figure 1b reported in literature*

Particle Type	**Particle Size (nm)**	**Saturation magnetization**	**Magnetic field gradient (T/m)**	**Length scale**	**Separation time**	**Reference**
Iron oxide nanoparticle	150 nm	N.A.	95.6 (max.)	~ 2 cm	4 minutes	[33]
Iron oxide nanoparticle	50 nm	N.A.	95.6 (max.)	~ 2 cm	~ 8 minutes	[50]
Bare Fe_3O_4	300 nm	74.61 emu/g	95.6 (max.)	1.8 cm	8 minutes	[51]
PSS-grafted Fe_3O_4	200 nm	70.99 emu/g	95.6 (max.)	1.8 cm	15 minutes	[51]

2.2 A simple analytical model for convective LGMS

Now our objective here is to modify the analysis presented in Section 2.1, which assumed that the fluid was at rest and only the particles were moving, in order to describe the

process shown in Figure 1b by including the convective motion of the fluid induced by the magnetic field. Let us consider a LGMS setup as shown in Figure 1b and Figure 3, where a cuvette filled with fix volume of MNPs solution is located on the top of a permanent cylindrical magnet (please refer to Supporting Information S2 or our early work[34] to understand why gravitational pulling is insignificant under this scenario). Under the influence of magnetic field generated by the permanent magnet, magnetophoresis is initiated and MNPs solution starts to flow convectively as a consequence of hydrodynamic interaction (see Figure 1b). Certain portion of MNPs that are impelled to the cuvette surface adjacent to the magnet (which is the inner wall at the bottom of cuvette such as the one shown in Figure 3) will be trapped and immobilized. Such a surface is the plane characterized by the strongest magnetic field and magnetic field gradient over the entire domain of MNPs solution undergoing magnetophoresis. In this work, we will designate this surface as the *MNPs collection plane*. Hereof, the MNPs collection plane can be visualized as a plane where MNPs are withdrawn from the solution. Nonetheless, only fraction of MNPs are being captured from the MNPs solution and immobilized after making physical contact with the MNPs collection plane. Due to the continuity nature of the fluid flow, the convective flow which is directed towards the collection plane (magnetic field source) will be circulated back to the suspension media.[52] This process keeps repeating until all the MNPs are captured on the collection plane. The circulating flow is the main reason for the continuous homogenization of MNPs throughout the entire solution.[34] It is important to emphasize that both experiments and computer simulations (simulations including a full hydrodynamic description using Navier-Stokes equations, see Ref[34]) show the presence of convective rolls and the uniformity of the MNPs solution throughout the magnetophoresis process of the kind shown in Figure 1b. Examples of typical velocity profiles and concentration profiles obtained in hydrodynamic simulations are given in the Supporting Information S3. Due to the uniformity of MNPs solution contributed by the continuous

homogenization of magnetophoresis induced convective flow,[34] the entire domain within the MNPs solution is having the same MNPs concentration c which is only a function of time t.

$$c = c(t) = \frac{N(t)}{V} \ , \tag{4}$$

where $N(t)$ is the number of particles in dispersion and V is the volume of the MNPs solution subjected to magnetophoresis. The vertical flux of particles J_z (per unit time and surface area), is given by:

$$J_z(z,t) = -v_z(z,t)c(t) \ , \tag{5}$$

where v_z is the z-component of the velocity of the particles. This vertical velocity of the particles can be written as the sum of two contributions, one due to the direct effect of the magnetic field gradient (the magnetophoretic velocity $v_m(z,t)$ given by Equation (3)) and another contribution due to the convective motion of the fluid $v_f(z,t)$:

$$v_z(z,t) = v_f(z,t) + v_m(z,t) = v_f(z,t) + \frac{d^3M}{18d_H\eta}\frac{\partial B}{\partial z} \tag{6}$$

The convective flow is strongly dependent on the MNPs concentration and magnetic field gradient, provided the geometry configuration and operating temperature remain the same.[34] Far from the magnet, the magnetic gradient is small and the motion of the particles is due to the fluid convective motion. On the contrary, near the collection plane the magnetic gradient is larger and the motion of the particles is mostly due to the effect of the direct magnetophoretic force (Equation (1)). In particular, at the collection plane ($z = 0$), the vertical velocity of the fluid is zero due to the impenetrability of the surface (the fluid cannot enter into the surface), so $v_f(z = 0, t) = 0$. By using this boundary condition in Equation (6), we obtain the value of the particle velocity at $z = 0$:

$$v_z(z=0) = \frac{m_s}{3\pi\eta d_H}\frac{\partial B}{\partial z}\Big|_{z=0} = \frac{d^3 M_S}{18 d_H \eta}\frac{\partial B}{\partial z}\Big|_{z=0} \quad (7)$$

In Equation (7), the magnetization of the particle (which depends on the applied field) has to be evaluated taking into account the magnetic field at $z = 0$. For typical magnets, the magnetic field at $z = 0$ is large enough so that the magnetization of the particles can be considered to be at magnetic saturation ($M \approx M_s$). Now, we can obtain the time evolution of the concentration as a function of time. The number of particles reaching the collection plane ($z = 0$) per unit time and unit surface area can be obtained by substituting Equation (7) into Equation (5). Therefore, the number of particles reaching the collection plane per unit time is given by:

$$I_{MNP}(t) = A_S v_z(z=0)c(t) = A_S \frac{M_S d^3}{18\eta d_H}\frac{\partial B}{\partial z}\Big|_{z=0} c(t) \quad (8)$$

where A_s is the area of the collection plane. A substantial fraction of MNPs that are reaching the collection plane will be captured, immobilized and separated from the MNPs solution. The remaining MNPs will be redispersed back to the solution by the convective current as the consequence of viscous drag and circulate throughout the solution before their immobilization on the MNPs collection plane. Under this scenario, we define the MNPs capture fraction f (on a particular MNPs collection plane) as the probability in which MNPs are successfully separated from the solution after making physical contact with the given collection plane. Consequently, the separation rate of MNPs (or MNPs capture rate) at any given time t, $I_c(t)$ can be formulated as:

$$I_c(t) = f I_{MNP}(t) = f v_z(z=0) A_s c(t) \quad (9)$$

In Equation (9), $f = 1$ corresponds to a 100% capture of all particles reaching the collection plane, whereas $f = 0$ corresponds to the complete redispersion of MNPs into the solution after contacting with the collection plane (no capture of particles).

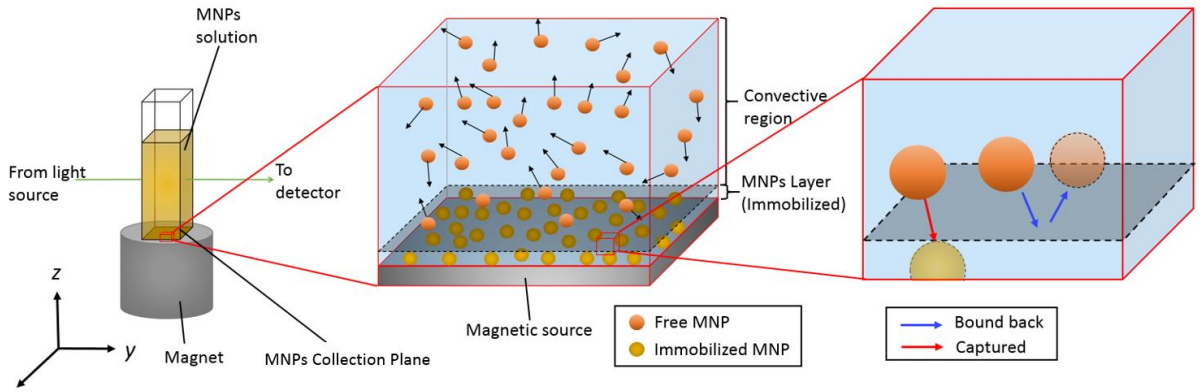

Figure 3*. The experimental setup of LGMS used in current study. A cuvette filled in MNPs solution was positioned on top of a cylindrical magnet such that MNPs were continuously captured and immobilized on the cuvette's bottom wall (which is the MNPs capture plane under this arrangement). The figure on the right hand side illustrates the hypothesized picture of LGMS when magnetophoresis induced convection is significant. MNPs suspended in the solution were driven by the convective current and they will reach MNPs collection plane after some time. Portion of these MNPs will be immobilized and form MNPs layer on the collection plane (red arrow). However, some of them will be driven back to the solution by the convective current after making physical contact with the collection plane (blue arrow).*

Due to the continuous withdrawal of MNPs at the collection plane, the number of MNPs within the solution decreases in tandem with time advancement. The kinetic of the magnetophoresis process can be written as follows:

$$\frac{dN(t)}{dt} = -I_c(t) \tag{10}$$

where $N(t)$ is the number of MNPs that are still suspended and remained in the MNPs solution at any given time t. By inserting Equations (4) and (9) into Equation (10),

$$\frac{dc(t)}{dt} = -\frac{f v_z(z=0) A_s c(t)}{V} \tag{11}$$

Here, we define the product of MNPs capture fraction f, the normal component of MNPs solution flow velocity at the collection plane (which is v_z in the current geometry arrangement) and area of MNPs collection plane A_s as separation factor α:

$$\alpha = f v_z(z=0) A_s \tag{12}$$

By incorporating Equation (7) into Equation (12), the following expression is obtained:

$$\alpha = \frac{1}{18} f \left(\frac{M_s d^3}{\eta d_h}\right) A_s \left.\frac{\partial B}{\partial z}\right|_{z=0} \tag{13}$$

In accordance to Equation (13), it can be deduced that the separation factor α is dependent on three elements: (1) properties of MNPs solution subjected to magnetophoresis (which are volumetric magnetization of MNPs, MNPs core diameter, MNPs hydrodynamic diameter and viscosity of the MNPs solution), (2) area of the MNPs collection plane and (3) normal component of magnetic field gradient on the MNPs collection plane. On the contrary, this separation factor α is independent of the MNPs concentration, amount (or volume) of MNPs solution used in any given magnetophoresis process as well as fluid flow velocity within the MNPs solution. The higher separation factor will lead to the faster magnetophoretic collection of MNPs from the solution and shorten the time required to attain certain level of separation. Even through the separation factor α is independent of fluid velocity adjacent to the MNPs collection plane $v_f(z \to 0)$, the hydrodynamic interaction plays a predominant role in the dynamical behavior in LGMS due to its homogenization effect. The generation of convective current (as a result of hydrodynamic effect) creates uniformly distributed MNPs solution throughout the entire timescale of magnetophoresis and this is the most important assumption in this model.

In accordance to Equation (11), batchwise LGMS system (where fixed volume of MNPs solution is exposed to a steady external magnetic field generated by permanent magnet) obeys the first order kinetic as follows:

$$\frac{dc(t)}{dt} = -kc(t) \tag{14}$$

where the rate constant k is given by:

$$k = \frac{f v_z(z=0) A_s}{V} = \frac{\alpha}{V} \tag{15}$$

The rate constant k in Equation (15) is time invariant because of two reasons. Firstly, the three elements that affect the separation factor α, as stated above, remain unaltered during the whole magnetophoresis process. Secondly, the volume of MNPs solution subjected to magnetophoresis V is also unaffected as time progresses because MNPs solution is not supplied nor removed from the system throughout the entire batchwise process. Correspondingly, the time-varying MNPs concentration $c(t)$ in batchwise LGMS can be approximated as a simple first order kinetic as shown in Equation (14).

The integration of Equation (14) gives:

$$\ln \frac{c(t)}{c_o} = -kt \tag{16}$$

where c_o is the initial concentration of the MNPs solution. Thus, $\frac{c(t)}{c_o}$ is the normalized concentration of MNPs solution which ranges from 0 (blank sample) to 1 (initial MNP concentration). According to Equation (16), the plot of $\ln \frac{c(t)}{c_o}$ against t should be a straight line passing through the origin with slope $-k$ if the hypothesized mechanism is accurate.

On the other hand, the inversion of Equation (15) gives:

$$\tau = \frac{1}{k} = \frac{1}{\alpha} V = \frac{1}{f v_z(z=0)} \frac{V}{A_S} \tag{17}$$

where τ is the time constant for a particular LGMS process. Hence, by using the same MNPs solution (the volumetric magnetization and size of MNPs as well as the viscosity of the solution are identical) and geometrical configuration (total area of MNPs collection plane and magnetic field distribution remain unchanged) to perform LGMS, the reciprocal of rate constant k (or time constant τ) is directly proportional to the volume of MNPs solution. In other words, the rate constant k of the extinction profile of magnetophoresis declines with the volume of MNPs solution subjected to LGMS as longer time is required for larger volume of MNPs solution to achieve certain degree of separation.

The predictions of the model can be now compared with published experimental results. For example, for the experiments reported in our previous work,[34] Equation (7) predicts $v_z \approx 7.8 \times 10^{-7}$ m/s (we consider $d \approx d_H \approx 31$ nm, $\eta \approx 10^{-3}$ Pa·s, and a magnetic gradient of ~100 T/m at the collection plane). By taking into account this predicted vertical velocity, now we can obtain the kinetics of the magnetophoretic process by assuming a perfect efficiency of $f = 1$ and noting that the experimental cuvette has $\frac{V}{A} = 3$ mm. Perfect efficiency of $f = 1$ is assumed as magnetic dipole-dipole attraction energy is about 2.7 times higher than the thermal energy possessed by each MNP to overcome the magnetic attraction (Please refer to Supporting Information S4 for more detailed justification of this assumption). By plugging in these values into Equation (17), we predict $\tau^{-1} \approx 1.57 \times 10^{-3}$ min^{-1}. This result is in very good agreement with the experiments reported in Ref[34], in which the concentration was observed to decay exponentially with a decay constant of $k = \tau^{-1} \approx 1.52 \times 10^{-3}$ min^{-1} as obtained from the linear fit of the experimental data.

Now, our purpose for the remaining of the paper is to perform an extensive test of the magnetophoretic model proposed in this section by analyzing experiments performed under different conditions (different volume of MNPs solution V, different magnetic field gradient $|\nabla B|$ and different MNPs size). Before considering the experimental tests of Equations (7) – (17), a technical detail has to be taken into account. In the derivation of the model, we assumed that the magnetic gradient depends only on z, being uniform at the collection plane. However, in typical experimental setups, the magnetic field gradient is not uniform on the collection plane. In order to take this effect into account in Equations (7), (8) and (13), the $A_s \left.\frac{\partial B}{\partial z}\right|_{z=0}$ term is substituted by the average of $\langle\frac{\partial B}{\partial z}\rangle_S$ over the entire collection plane:

$$A_S \langle\frac{\partial B}{\partial z}\rangle_S = \iint_S \left.\frac{\partial B}{\partial z}\right|_{z=0} dA. \tag{18}$$

while S is representing the MNPs collection plane. Here, we assumed the MNPs collection plane is located at the bottom, inner surface of the cuvette where the magnetic field gradient is the highest within the system (remember that the space occupied within the wall thickness contribute the largest magnetic field gradient drop). For the experiments reported in this paper, as standard cuvette is used, the MNPs collection plane is of the square shape and has the dimension of 1 × 1 cm. Yet, the surface integral in Equation (18) can be further simplified due to the axial symmetry of magnetic field produced by the cylindrical magnet. The magnetic field gradient $\frac{\partial B}{\partial z}$ in a particular point on the collection plane is only the function of the displacement from the magnet axis r. Also, by assuming the center of the square-shaped MNPs collection plane (with side length of $2R$) is overlapping with the axis of the cylindrical magnet, Equation (18) can be further simplified to:

$$A_s \langle\frac{\partial B}{\partial z}\rangle_S \cong \int_{r=0}^{r=\sqrt{2}R} \frac{\partial B}{\partial z}(r)\, dA(r) \tag{19}$$

where $dA(r)$ is given by:

$$dA(r) = \begin{cases} 2\pi r\, dr, & 0 < r \leq R \\ 2r\left(\pi - 4\cos^{-1}\frac{R}{r}\right) dr, & R < r \leq \sqrt{2}R \end{cases} \quad (20)$$

The simplification of Equation (18) into Equations (19) and (20) according to the assumptions stated is demonstrated rigorously in Appendix A2. The z-derivative of magnetic field strength B as the function of r, $\frac{\partial B}{\partial z}(r)$ can be numerically calculated by Biot-Savart law by using MATLAB.

3. Experimental Materials and Methods

3.1 Materials

Magnetic nanoparticles (MNPs) used in this study were purchased from Ocean NanoTech which are made up of the suspension of polyethylene glycol (PEG) coated magnetite (Fe_3O_4) spherical nanoparticle in aqueous media. There were two different core size of MNP being used in this study: (1) 30 nm (SMG-30) and (2) 20 nm (SMG-20).

3.2 Characterization of MNPs

Transmission electron microscopy (TEM). Prior to the TEM analysis, a droplet of MNPs solution (approximately 30 μL) with concentration of 50 mg/L was transferred onto a carbon coated TEM grid. After three minutes of waiting time, sufficient amount of MNPs had been deposited on the grid and the grid was then left sitting on a piece of filter paper for air drying. Next, MNPs on the grid were observed with TEM (JEOL, JEM-20CX).

Dynamic light scattering (DLS). The received MNPs solution (which has concentration of 1000 mg/L) was diluted to 10 mg/L with deionised (DI) water. DI water employed was obtained from Elga Purelab Flex water purification system with resistivity of 18.2 MΩ. The purpose of dilution was to reduce the multiple scattering effect and MNPs interaction within the solution throughout the measurement.[53] The diluted MNPs solution was then gleamed with a light beam and the scattered light intensity was measured at an angle of 173º to the incident light. The transient light intensity fluctuation was recorded and fitted into a correlation function. The correlation function decay rate served as an indicator for the intensity of diffusion of MNPs that are suspended in the solution. The faster decay rate reflects the faster diffusion of MNPs and hence higher translational diffusivity. The cumulant method was used to deduce the translational diffusivity of MNPs according to the correlation function. Finally, based on the translational diffusivity, the hydrodynamic size of MNPs in the solution was calculated by using Einstein-Stokes equation.

Vibrating sample magnetometer (VSM). Three mL of as-received MNPs solution was dispersed in DI water and transferred to a spherical flask. The sample was then cooled down to -5 ºC to freeze the solution. Next, the sample was connected to a freeze dryer for 24 hours. MNPs in powder form was obtained and 0.0006 g of the dried MNPs was dispersed in an epoxy to form a cast epoxy sample which was then attached to a vibrating glass rod at the centre of an electromagnetic direct current field. The response of MNPs towards the magnetic field was measured for both the positive and negative field components with digitally controlled field stepping and data averaging (ARkival ADE/DMS Model 880).

3.3 Magnetophoresis kinetics measurement

The magnetophoresis experimental setup is shown in Figure 3 as similar to our previous work.[34] Prior to the kinetics measurement, the as-received MNPs solution (which has concentration of 1000 mg/L) was diluted to 20 mg/L. Next, 1 mL of diluted MNPs solution was transferred to a standard size 1 × 1 × 4 cm polystyrene disposable cuvette (Malvern, DTS0012). The cuvette filled with diluted MNPs solution was placed on top of a cylindrical permanent magnet. Here, we used NdFeB permanent magnet which radius and height are 0.7 cm and 1.5 cm, respectively (denoted by NdFeB1 magnet in this study). NdFeB1 magnet was purchased from Ningbo YuXiang E&M Int' l Co, Ltd and N-50 graded with remanent magnetization of 1.45 T. Under the influence of the magnetic field generated by the permanent magnet, magnetophoresis was initiated and concentration of MNPs begin to decline as time progressed due to the continuous collection of MNPs. In this regard, UV-vis spectrometry (Agilent Cary-60) was used to obtain the extinction profile of MNPs solution that is undergoing magnetophoresis. Here, monochromatic light was passed through the MNPs solution and light absorbance was recorded every 5 minutes after the initialization of magnetophoretic collection. As the Beer-Lambert's law was proven to be accurate within the MNPs concentration encountered in this study (see Supporting Information S5 for justification), linear relationship between MNPs concentration and light absorbance is assumed such that the normalized concentration of MNPs solution could be calculated by the following equation:

$$\frac{c(t)}{c_o} = \frac{A(t) - A_0}{A_i - A_0} \tag{21}$$

where $A(t)$ is the light absorbance of MNPs solution in any given time t, A_0 is the light absorbance of blank solution and A_i is the light absorbance of MNPs solution before undergoing magnetophoresis. The procedure above was repeated by subjecting different volume of MNPs solution to magnetophoresis: 1.5 mL, 2.0 mL, 2.5 mL and 3.0 mL.

Next, the magnetophoresis experiment elaborated above was repeated by adding spacers of different height between the magnet and the cuvette, using different magnets (NdFeB1, NdFeB2, NdFeB3 and SmCo magnets, described in Table S1 in Supporting Information S6) and changing the MNPs size (SMG-20 and SMG-30). The conditions of all the experiments are summarized in Table 2.

Table 2*. Experiments performed in this work for a 1 × 1 × 4 cm cuvette filled with a MNPs solution at concentration of 20 mg/L. Each experiment is repeated at different solution volumes: 1.5 mL, 2.0 mL, 2.5 mL and 3.0 mL. Magnet properties are described in Figure 4 and Table S1 in Supporting Information.*

Experiment	Magnet	Spacer (mm)	Particles
A	NdFeB1	0	SMG-30
B	NdFeB1	2.5	SMG-30
C	NdFeB1	5.0	SMG-30
D	NdFeB2	0	SMG-30
E	NdFeB3	0	SMG-30
F	SmCo	0	SMG-30
G	NdFeB1	0	SMG-20

In Experiments B and C the spacer is included to change the magnetic field gradient on the collection plane (the thicker the spacer is the lower the magnetic field gradient on the MNPs collection plane becomes). Experiments A, D, E and F correspond to the use of different magnets and hence different combinations of magnetic field gradients at the MNPs collection plane and different decays inside the dispersion. Finally, experiment G corresponds to the use of particles with a smaller size. The 2D plot of magnetic field gradients produced by the all magnets mentioned above (NdFeB1, NdFeB2, NdFeB3 and SmCo) at different elevations are

reported in detail in the Supporting Information S7. Here we report the profiles of average magnetic field gradient $< \frac{\partial B}{\partial z} >$ (across the cross sectional surface within the 1 × 1 × 4 cm disposable cuvette filled with MNPs solution) against the distance from magnet which is calculated by Equations (19) and (20) by using MATLAB (Figure 4). We also indicate in Figure 4 the location of the MNPs collection plane, which in the absence of spacer we consider it to be at a displacement of 0.165 cm (thickness of the cuvette bottom wall or elevation of MNPs collection plane from the magnetic pole in these experiments) away from the magnet surface (please refer to Appendix A3 for more detailed calculation of the displacement of the MNPs collection plane from the magnet pole). The profiles shown in Figure 4 are important to understand the differences between experiments A to F. In experiments A, B and C we employ the same magnet (NdFeB1) but the magnetic field gradient at the collection plane is different due to the presence of spacer (see Figure 4). The different neodymium boron ferrite magnets of different dimension considered in experiments A, D and E (NdFeB1, NdFeB2 and NdFeB3) share the same remanence magnetization at 1.45 T but produce different magnetic field gradients as shown in Figure 4. Therefore, according to our calculation, NdFeB1 and NdFeB2 magnets exert nearly similar $< \frac{\partial B}{\partial z} >$ on the MNPs collection plane, which was given by 111.2 and 108.9 T/m respectively. On the contrary, NdFeB3 magnet give lower $< \frac{\partial B}{\partial z} >$ on the MNPs collection plane at 75.4 T/m, even though it was made up of larger magnetic volume compared to NdFeB1 and NdFeB2 magnets. Ironically, the weaker SmCo magnet employed in experiment F, which has the same dimension with that of NdFeB1 magnet provides almost similar magnitude of magnetic field gradient on the MNPs collection plane (~74.6 T/m) with that of NdFeB3 magnet of experiment E.

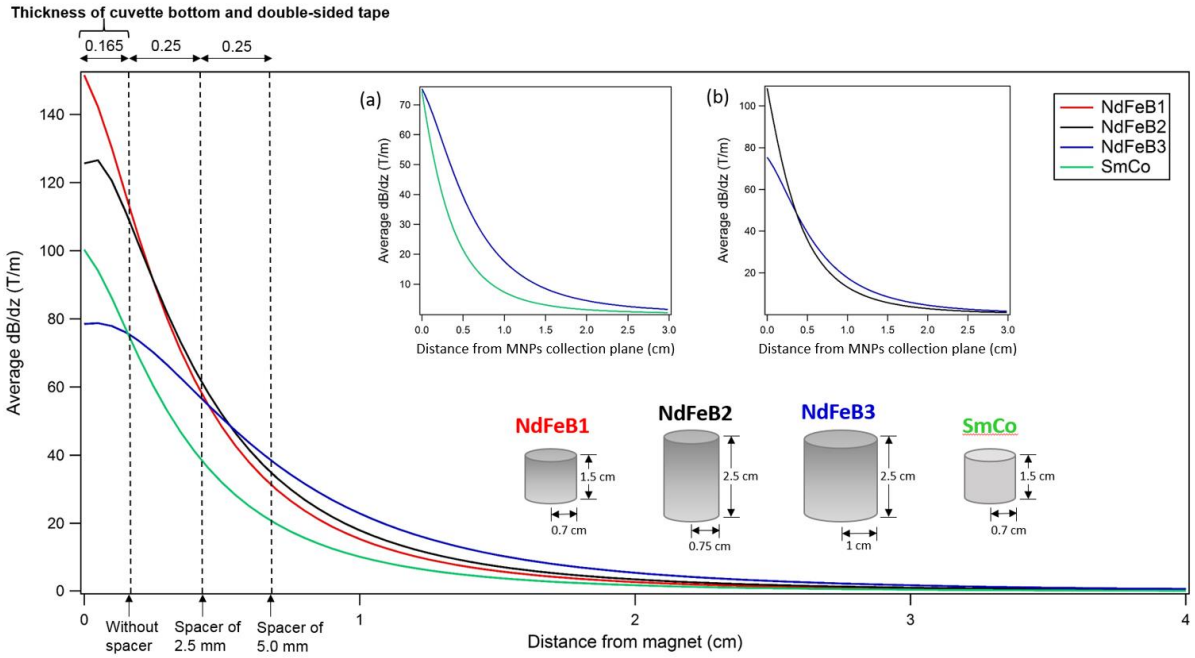

Figure 4*. The plot of average magnetic field gradient against distance from magnet pole for four types of permanent cylindrical magnets employed in the current study (NdFeB1, NdFeB2, NdFeB3 and SmCo). The dotted lines indicate the position of MNPs collection plane for the following cases: (i) without spacer (the displacement between the MNPs collection plane and magnet pole is solely contributed by the thickness of cuvette bottom wall and double-sided tape), (ii) with spacer of 2.5 mm in between the magnet pole and the cuvette, (iii) with spacer of 5.0 mm in between the magnet pole and the cuvette. Inset: Comparison of average magnetic field gradient imposed on the MNPs solution (with V = 3 mL) by (a) NdFeB3 and SmCo magnets; (b) NdFeB2 and NdFeB3 magnet. Additionally, please refer to Supporting Figure S4 for magnetic field gradient profile across the MNPs solution for Experiments B and C (NdFeB1 magnet with spacer of 2.5 mm and 5.0 mm).*

4. Results and discussion

4.1 Characterization of MNPs

As demonstrated in Figures 5a & 5b, both SMG-20 and SMG-30 consist of aqueous suspension of MNPs that are almost spherical in shape. Furthermore, these particles are virtually uniform in size and has relatively low polydispersity. Evidently, based on the image analysis by using ImageJ on 100 randomly selected MNPs, the core diameter of MNPs from SMG-20 and SMG-30 are given by 18.33 ± 1.08 nm and 30.94 ± 2.18 nm, respectively. On the other hand, Figures 5c & 5d illustrate the hydrodynamic size distribution of particle system obtained from SMG-20 and SMG-30, as measured by DLS. The zeta average of hydrodynamic diameter for particle system originated from SMG-20 and SMG-30 are given by 31.21 nm and 45.47 nm respectively. The hydrodynamic diameter measured by DLS is slightly greater than the MNPs core diameter observed under TEM as PEG coating on the MNP is also contributing to the hydrodynamic diameter. According to core diameter and hydrodynamic diameter measured, the thickness of the coating layer is estimated to be 6.44 nm for SMG-20 and 7.27 nm for SMG-30. This results have justified the information provided by the supplier which states that the polymer thickness is around 6 nm for both samples (SMG-20 and SMG-30).[54] Figures 5e & 5f show magnetization curve for MNPs which make up SMG-20 and SMG-30. MNPs from both samples exhibit superparamagnetic property due to the insignificant hysteresis loop in the magnetization curves. Besides, the saturation magnetization of MNPs from SMG-20 and SMG-30 are almost similar, at 46.43 emu/g and 42.79 emu/g, respectively. The slight difference in the saturation magnetization between MNPs obtained from both given sample is most probably contributed by their dissimilarity in the mass ratio of PEG coating to MNPs core.

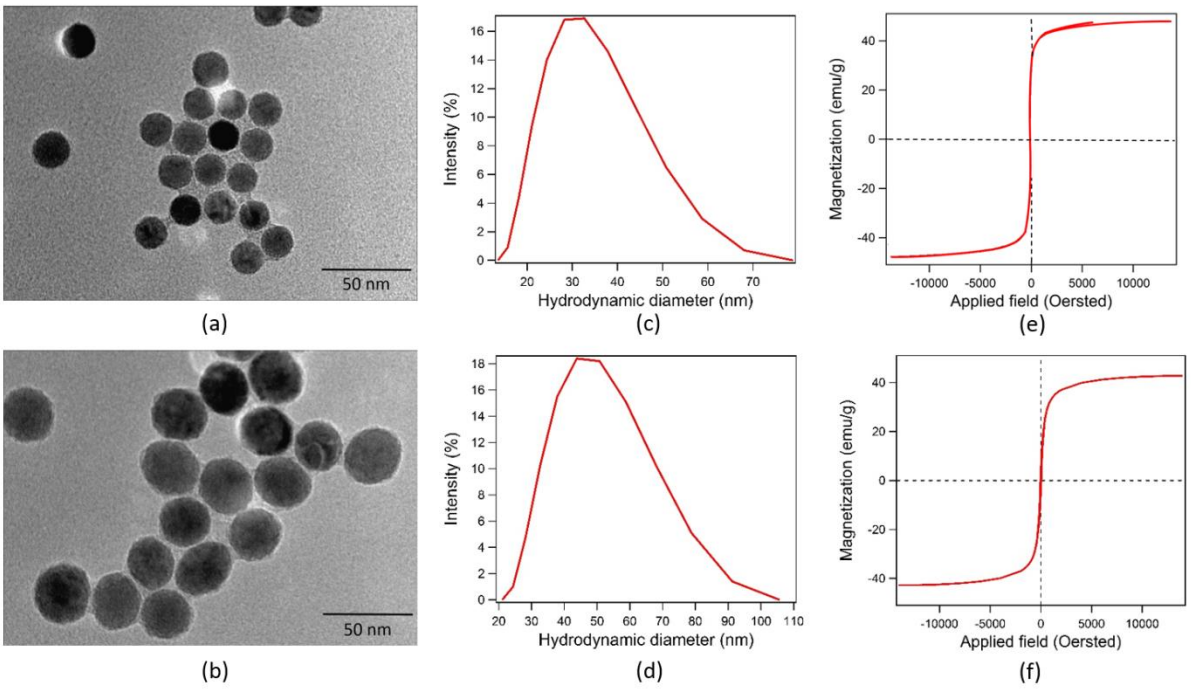

Figure 5*. TEM images of (a) SMG-20 and (b) SMG-30, hydrodynamic diameter distribution of (c) SMG-20 and (d) SMG-30, and, magnetization curve of (e) SMG-20 MNPs and (f) SMG-30 MNPs. Results presented in (c) and (d) are from DLS measurement, while (e) and (f) are from VSM measurement.*

4.2 Magnetophoresis kinetics

First, let us consider the results of Experiment A (see Table 2), in order to characterize the kinetics of LGMS under a permanent cylindrical magnet and perform a quick test on the theory presented in Section 2.2. In this experiment, we considered magnetophoresis of MNPs (SMG-30) solution with different volume under the influence of magnetic field generated by NdFeB1 magnet. Figure 6a shows the obtained extinction profiles which demonstrate that the normalized concentration of MNPs solution decreases with time once magnetophoresis is initiated. The external magnetic field exerts magnetophoretic force to each MNP and drive MNPs towards the magnet. Eventually, almost all suspended MNPs are captured on the

collection plane and the MNPs concentration fall to virtually zero at the end of the experiment. Also, as demonstrated in Figure 6a, MNPs solution with larger volume requires much longer time to achieve certain level of separation compared to those with smaller volume. For instance, 430 minutes are needed for 1 mL of MNPs solution to achieve 99% of MNPs removal while 3 mL of MNPs solution requires 1820 minutes to achieve the same level of separation. As shown in Figure 6b all separation profiles obey first order kinetic with great precision as the plot of $\ln\frac{c(t)}{c_o}$ against separation time t could be fitted almost exactly into a straight line passing through the origin (with coefficient of determination $R^2 > 0.98$ for all cases) regardless of the volume of MNPs solution employed. Therefore, the kinetic behavior of magnetophoresis process under low field gradient in current study agrees with Equation (16) up to an excellent accuracy while the decay rate constant k remains invariant as time progresses for all cases. As observed from Figure 6b, the value of k (which is the slope of $\ln\frac{c(t)}{c_o}$ against t) decreases as the volume of MNPs solution increases. This implies that the time constant $\tau = 1/k$ is observed to increase with the volume V, as expected from Equation (17). Figure 6c shows that this dependence is linear, as predicted by Equation (17). The inverse of this proportionality factor gives the separation factor α (see Equation (15)), which can be both determined experimentally and predicted theoretically. Using the values of the parameters for experiment A in Equation (13) and assuming a perfect efficiency of the LGMS process ($f = 1$), we predict $\alpha \approx 8\times10^{-3}$ mL/min. This prediction is in good quantitative agreement with the experimental result obtained from the linear fit presented in Figure 6c, which gives $\alpha = 1/122.8 \approx 8.14\times10^{-3}$ mL/min. Therefore, we can conclude that the model presented in Section 2.2 is in agreement with the results of experiment A.

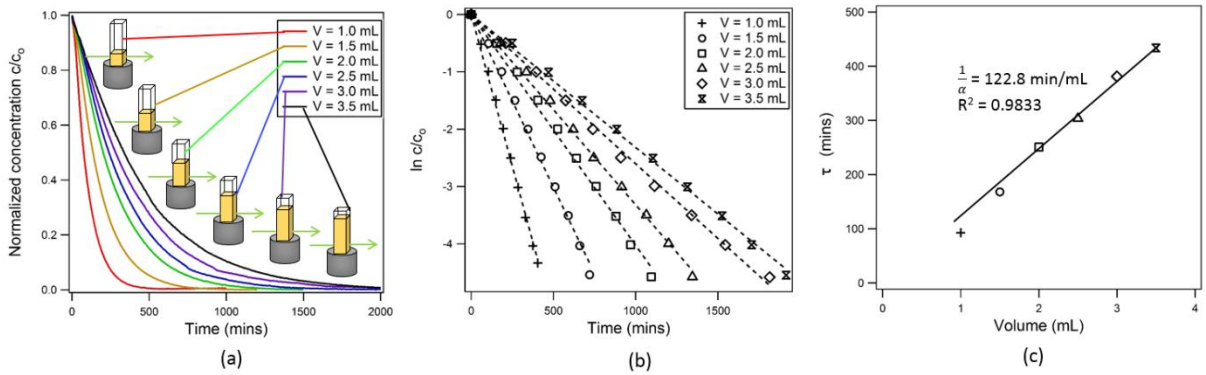

***Figure 6**. (a) Extinction profiles showing separation kinetic of different suspension volume of 20 mg/L MNPs solution (SMG-30) undergoing magnetophoresis under the magnetic field exerted by NdFeB1 magnet (Experiment A). (b) $ln\frac{c(t)}{c_o}$ versus t graphs for separation kinetic profiles shown in (a). Dotted lines are the linear fitting lines. The coefficient of determination R^2 and gradient k of the curve (by making simple linear regression) are tabulated in Table S2 in the Supporting Information. (c) τ against V graphs for Experiment A. The slope of the linear fitting line is the reciprocal of separation factor α.*

Now, we will analyze the effect on the kinetics of changing experimental conditions in different ways. In these experiments (see Experimental section for full details) we consider: the effect of changing the magnetic field gradient at the collection plane by adding a spacer between the cuvette and the same magnet employed so far (experiments B and C), the effect of changing the magnets with different dimension and thus the magnetic field profiles (experiments D, E and F) and finally the effect of employing particles with different size (experiment G). In all experiments we considered different MNPs solution volumes V. The separation kinetic profiles recorded from these experiments are given in the Supporting Information S8. All separation kinetics profiles and $\ln\frac{c(t)}{c_o}$ versus t graphs for different volumes V of the solution (Figures S5 to S10) obey the dependence predicted by Equation (16)

up to high accuracy with coefficient of determination R^2 greater than 0.95 (Please refer to Table S2 in Supporting Information). The magnetophoretic characteristic times $\tau = 1/k$ obtained from a fit to Equation (16) of all the experiments are given in Figure 7. In all cases, τ shows a linear dependency with the volume V, as predicted by Equation (17). Therefore, with a linear fit of τ versus V we can determine the separation factor α (see Equation (17)) for each experiment. We will now analyze these results in more detail in the following subsections.

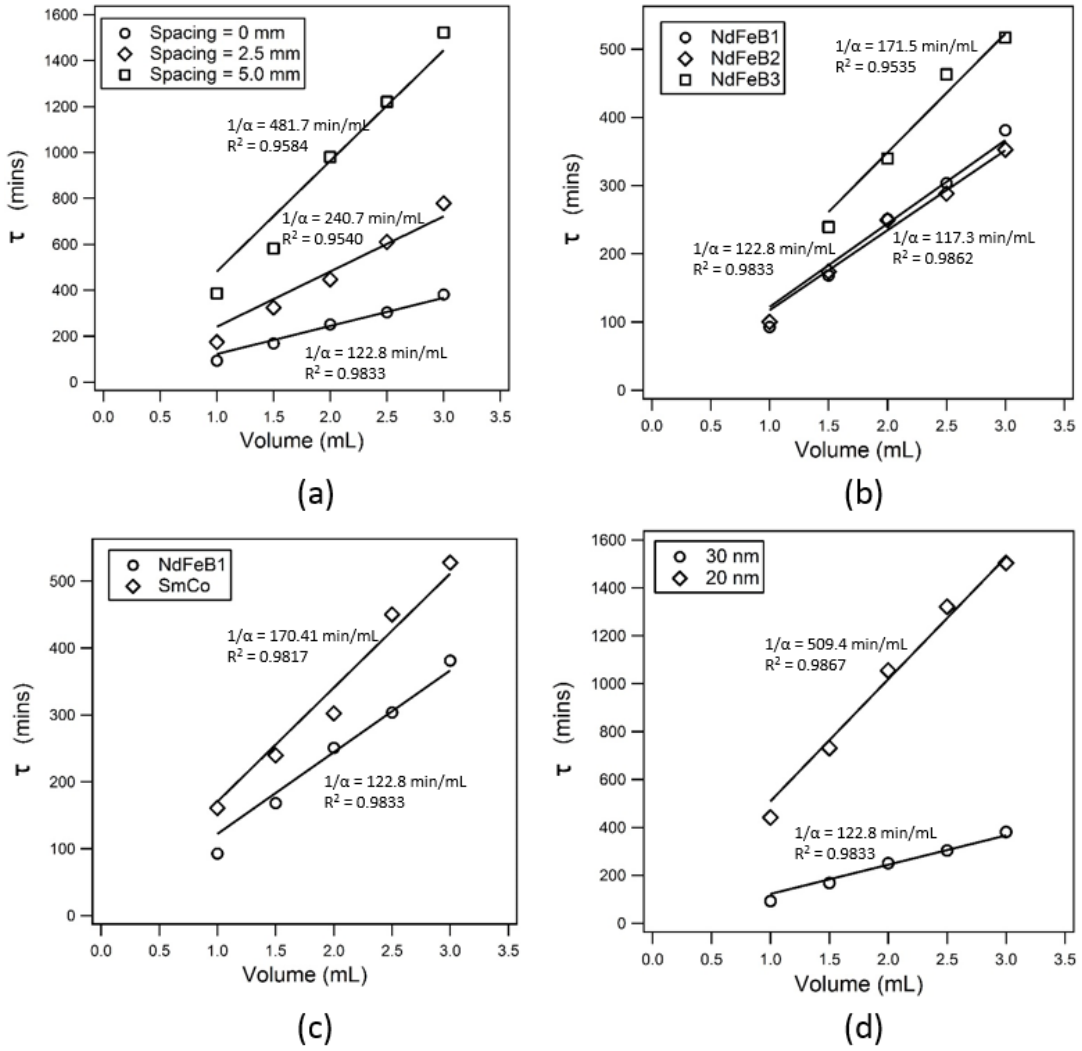

Figure 7*. Comparison of τ against V graphs for magnetophoresis experiments performed under different conditions. (a) 30 nm MNPs solution (SMG-30) with NdFeB1 magnet with different values of a spacer in between magnet and MNPs solution and without spacer*

(Experiments A, B and C), (b) SMG-30 with NdFeB1, NdFeB2 and NdFeB3 magnets (experiments A, D, E) , (c) SMG-30 with NdFeB1 and SmCo magnets (experiments A and F), (d) 20 nm MNPs solution (SMG-20) and SMG-30 with NdFeB1 magnet (experiments A and G).

4.3 Effect of magnetic field gradient at the collection plane on the magnetophoresis kinetics

The effect of magnetic field gradient at the collection plane on the magnetophoretic characteristic time τ can be seen in Figures 7a, 7b and 7c. Figure 7a shows the effect of adding a spacer between the cuvette and the magnet (experiments A, B and C) on the magnetophoresis kinetics. The figure shows that separation times increase as we decrease the magnetic field gradient at the collection plane by increasing the spacer length. We also obtain that the slope of τ against V (which is equal to the reciprocal of separation factor α) is steeper as the separation distance between magnet and MNPs solution increases (or equivalently, magnetic field gradient imposed on the MNPs collection plane decreases) (see Figure 7a). In Figure 7b, we compare the results of experiments performed by using three NdFeB magnets with different dimension (experiments A, D and E). According to Figure 7b, experiments A and D give very similar kinetics and experiment E gives slower kinetics. This phenomenon is because the magnets employed in experiments A and D exert almost the same magnetic field gradient at the collection plane whereas the magnet in experiment E has a lower value. In Figure 7c, we compare the results of experiment F (which employs a SmCo magnet) with that of experiment A. The separation factor α for experiment F (~0.0059 mL/min) is lower than that of experiment A (~0.0081 mL/min), so that the magnetophoretic collection rate is slower when samarium cobalt magnet is used instead of neodymium boron ferrite magnet even though both magnets have the same dimension. In this case, samarium cobalt magnet has the lower remanence

magnetization (~0.96 T) compared to neodymium boron ferrite magnet (~1.45 T) with less magnetic field gradient as well (Figure 4).

All these results discussed so far in Figures 7a to 7c are qualitatively consistent with the model predictions, since according to Equation (13) the separation factor α increases with increasing the value of the magnetic field gradient at the collection plane. In fact, we can see that experimentally this dependence is linear as predicted by Equation (13). This can be seen in Figure 8. Eventually, the experimentally obtained α values for all set of experiment are fitted quite well into a linear line passing through the origin with coefficient of determination R^2 given by 0.9837 (see Figure 8). This result agrees with Equation (13) which states that separation factor α is directly proportional to $< A_s \frac{\partial B}{\partial z} >$ on the MNPs collection plane.

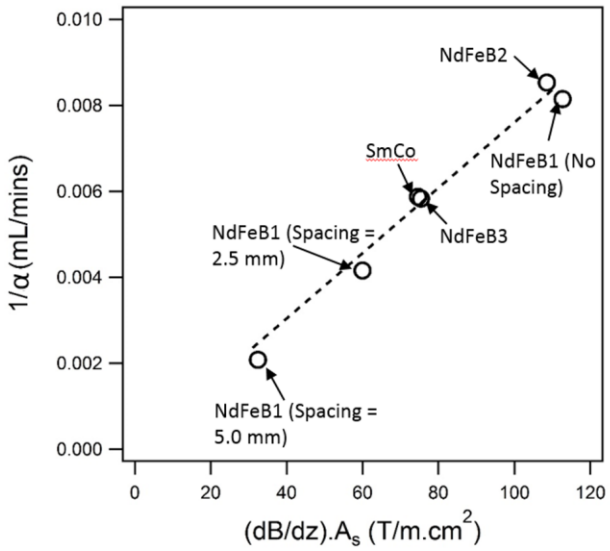

Figure 8. *The plot of α against $A_s \frac{\partial B}{\partial z}$ for magnetophoresis of SMG-30. The dotted line is the linear fitting line passing through the origin. The coefficient of determination R^2 of this fitting line is given by 0.9837. All values for α are calculated from results presented in Figure 7.*

4.4 Space dependency of magnetic field gradient is insignificant on influencing the kinetics of convection-dominant magnetophoresis

A very important result also obtained in Figure 8 is that the separation factor α is only dependent on the magnetic field gradient at the MNPs collection plane as shown in Equation (13) and completely independent from the spatial dependence of magnetic field gradient away from the collection plane within the MNPs solution. A particularly illustrative case is that of experiments E and F performed with NdFeB3 and SmCo magnets, respectively. In this case both magnets have almost identical magnetic field gradients at the collection plane but very different profiles of the magnetic gradient along the system (see Figure 4a). As seen in Figure 8, both have almost the same value of separation factor α. This is another important corroboration of the theory. In the classical model discussed in Section 2.1, the magnetophoretic velocity of MNPs is heavily dependent on the magnetic field gradient profile throughout the whole MNPs solution. However, for a magnetophoresis of a fixed volume of MNPs solution in which magnetically induced convection is a dominating phenomenon (the model presented in Section 2.2), the separation rate is only dependent on the total area of MNPs collection plane and the magnetic field gradient imposed on it. Subsequently, the magnetic field distribution across the MNPs solution is no longer playing a pivotal role in determining the magnetophoretic separation rate of MNPs if the magnetophoresis induced convection is overwhelming the magnetophoretic velocity of a single MNP.

In order to further illustrate this important result, we compare in more detail the results of experiments E and F for a particular MNPs solution volume (3 mL) in Figure 9a. The time evolution of the concentration is indistinguishable between both experiments. By comparing the magnetic field gradient profiles of NdFeB3 and SmCo magnets (Figure 4a), it can be observed that the magnetic field gradient generated by SmCo magnet decays much faster in comparison to that of NdFeB3 magnet even though the magnetic field gradient exerted by the

both magnets on the MNPs collection plane are almost similar in magnitude. Generally, at each points/plane beyond the collection plane, MNPs experience less magnetic field gradient and hence weaker magnetophoretic force when SmCo magnet (instead of NdFeB3 magnet) is employed in the magnetophoresis. So, the conventional magnetophoresis calculation of Section 2.1 predicts higher separation rate of MNPs for NdFeB3 magnet in comparison to that of SmCo magnet. Contrastingly, the model in Section 2.2 predicts equal separation rate for both magnets (NdFeB3 and SmCo). This observation has further verified our result that MNPs collection rate is only dependent on the magnetic field gradient at MNPs collection plane as demonstrated by the experimental result in Figure 9a.

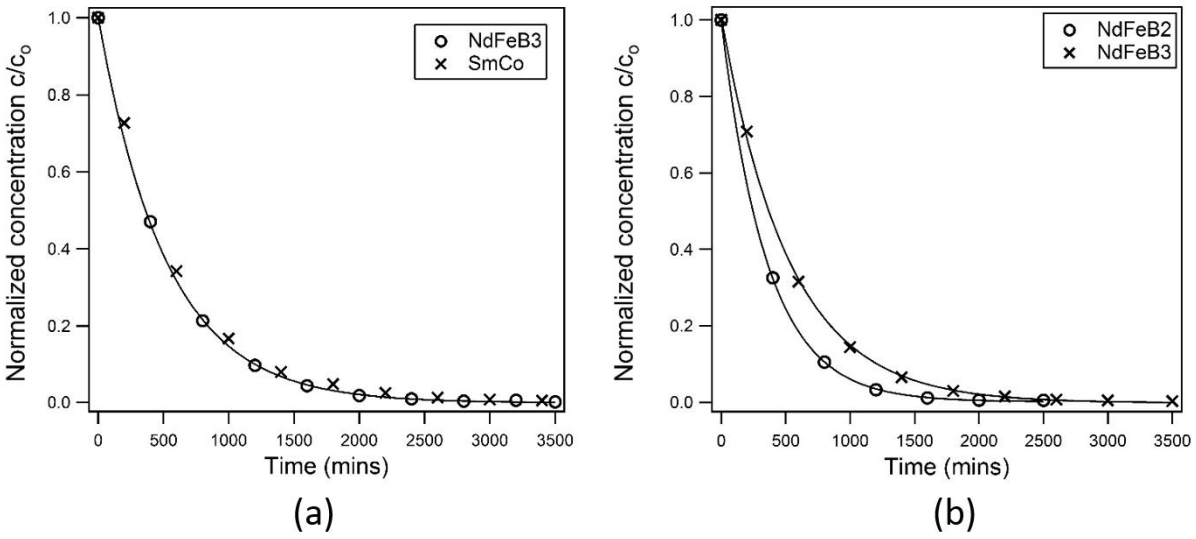

Figure 9*. The comparison of separation kinetic profiles for the magnetophoresis of 3 mL of 30 nm MNPs solution (SMG-30) by using (a) NdFeB3 and SmCo magnets; (b) NdFeB2 and NdFeB3 magnets.*

Additionally, the comparison between extinction profiles for LGMS which employs NdFeB2 and NdFeB3 magnets in experiments D and E (MNPs solution volume V = 3 mL) also

indicates that the magnetophoretic separation rate of 30 nm MNPs (SMG-30) is independent of the magnetic field distribution across the MNPs solution. As illustrated in Figure 4b, the average magnetic field gradient that is imposed by NdFeB2 magnet on the MNPs collection plane is higher in comparison to that of NdFeB3 magnet. However, due to its smaller size, magnetic field gradient generated by NdFeB2 magnet drops more rapidly with respect to distance from the magnet. For instance, magnetic field gradient produced by NdFeB2 magnet falls below that of NdFeB3 magnet when the distance from the magnet pole exceeds 0.4 cm (Figure 4b). As 3 mL MNPs solution filled in 1 × 1 × 4 cm disposable cuvette, the vertical height of the solution in the cuvette is 3 cm. In other words, as the MNPs solution is undergoing magnetophoresis (see arrangement shown in Figure 3), the separation distance between MNPs suspended in the solution and the MNPs collection plane ranges from 0 to 3 cm. Henceforth, more than 80% (vol %) of MNPs in the suspension experience lower magnetic field gradient and hence weaker magnetophoretic force when NdFeB2 magnet is used instead of NdFeB3 magnet. However, according to our experiment, NdFeB2 magnet induces more rapid magnetophoretic collection of MNPs in comparison to NdFeB3 magnet (Figure 9b). This result comes exactly as our mathematical model has predicted, since the magnetic field gradient exerted by NdFeB2 magnet on the MNPs collection plane is higher. Additionally, the magnetophoresis of 20 nm MNPs (SMG-20) shows the similar trend with the result demonstrated above (Please refer to Figure S11 in Supporting Information S9). In short, the rate of MNP collection under LGMS is independent of the magnetic field gradient (and hence magnetophoretic force on individual MNP) across the suspension as long as hydrodynamic effect is dominating and convective current has been generated within the solution.

4.5 Effect of particle size on magnetophoresis kinetics

The size of MNPs is also playing a vital role in governing the magnetophoretic collection rate of MNPs during LGMS. As demonstrated in Figure 7d, the separator factor α for 20 nm MNPs (SMG-20) at 0.0020 mL/min is approximately four times lower than those 30 nm MNPs (SMG-30) at 0.0081 mL/min. This result is also consistent with Equation (13), which predicts a strong dependence of the separator factor α with the hydrodynamic size of the particle, the size of the magnetic core and also with the magnetization (which is different for both kinds of particles). However, a more quantitative comparison it is not possible because of the large sensitivity of Equation (13) to these quantities which requires a more precise experimental characterization of the particles.

4.6 Geometry dependency of magnetophoresis

As clearly illustrated in Equations (13) to (18), the rate of magnetophoresis is dependent on the $A_s \frac{\partial B}{\partial z}$, and hence, this section investigate the effects of both A_s and $\frac{\partial B}{\partial z}$ on magnetophoresis. Figure 10a demonstrates the time lapse photos of MNPs solution subjected to magnetophoresis under magnetic field created by NdFeB1 and NdFeB3 magnets. The cuvette employed has the dimension of 2 × 2 × 4 cm (which is 4 times the volume of standard cuvette) and it was filled with 12 mL of 100 mg/L MNPs solution in this experiment. Under this setup, it allows us to evaluate the contribution of A_s, which is not possible to study by using a smaller cuvette in previous experiment (in former case, the magnets employed are nearly same size or larger than the cuvette and hence, the area of MNPs collection plane is the same for all experiments). According to this figure, the rate of magnetophoresis initiated by NdFeB3 magnet is slightly higher in comparison to that of NdFeB1 magnet. This statement has been supported by Figure 10b which demonstrates the increment of light (which passing

through the MNPs solution) intensity versus time graph. The light intensity through the MNPs solution was obtained by analyzing the given time lapse images with ImageJ (a freeware available online). Since MNPs suspended in the solution tend to absorb light that is penetrating through the solution, the light emitted from MNPs solution with higher concentration has the lower intensity. As illustrated in Figure 10b, the light intensity throughout the MNPs solution increases as time progresses is suggesting the concentration decrement of MNPs solution over time, regardless of the dimension of magnet being used. However, the light intensity of MNPs solution increases more rapidly when NdFeB3 magnet was employed. This observation has implied that magnetophoresis induced by NdFeB3 magnet is faster in comparison to that of NdFeB1 magnet under such configuration. In fact, this result is consistent with time lapse images of magnetophoresis which are demonstrated in Figure 10a.

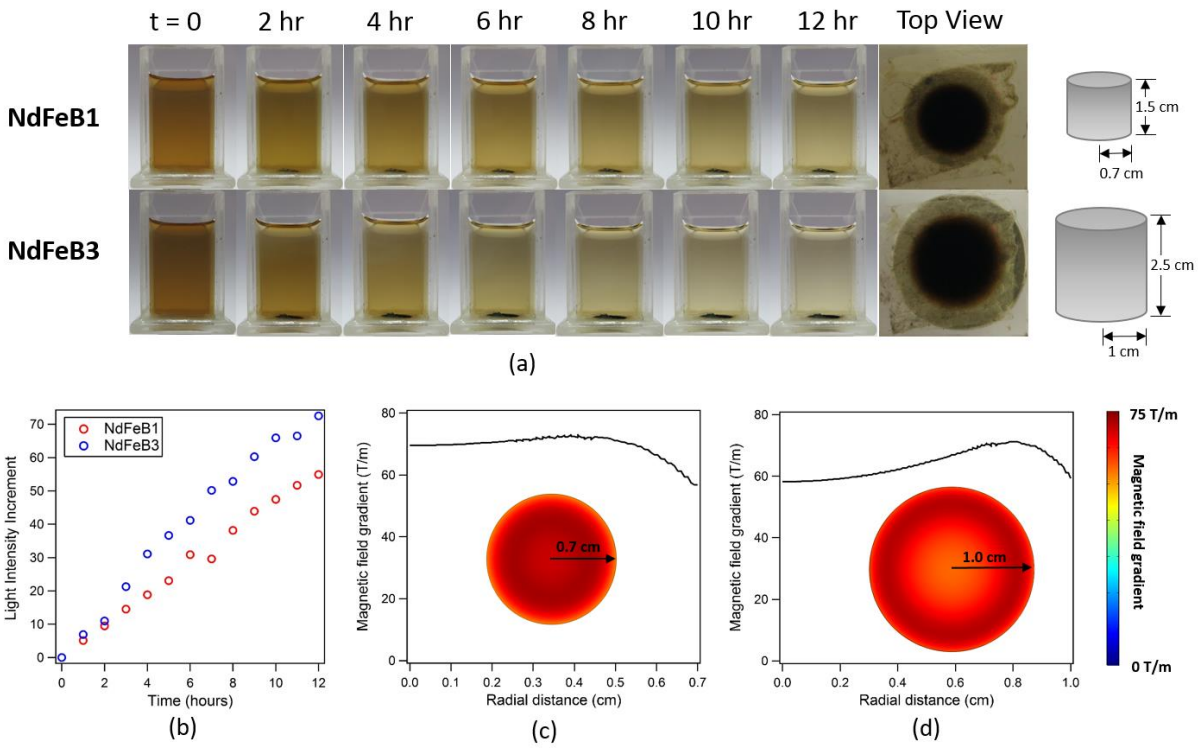

Figure 10. *(a) Time lapse photos for magnetophoresis of MNPs solution (SMG-30) by employing NdFeB1 and NdFeB3 magnets. The dimension of the cuvette is 2 × 2 × 4 cm and 12*

mL of 100 mg/L MNPs solution was filled in the cuvette to undergo magnetophoresis. The thickness of the cuvette, and hence the displacement between the MNPs collection plane and magnet pole, is 3.5 mm. The top view of the MNPs solution undergoing magnetophoresis for both cases are also illustrated. (b) The plot of light intensity increment against time for the magnetophoresis by employing NdFeB1 and NdFeB3 magnets. (c) Magnetic field gradient profile created by NdFeB1 magnet on the MNPs collection plane. (d) Magnetic field gradient profile created by NdFeB3 magnet on the MNPs collection plane. The inset in (c) and (d) show surface plot of magnetic field gradient for collection plane which is located at displacement of 3.5 mm from the magnet pole. The full profile of 2D magnetic field gradient plot with respect to separation distance from the magnet is available in Supporting Information S7.

Yet, this observation seems inconsistent with the experimental result presented in Figure 7b which shows that NdFeB1 magnet induced faster magnetophoretic collection rate of MNPs in comparison to that of NdFeB3 magnet. In order to understand the difference between both experiments, we have to take into account two factors. Firstly, the cuvette employed in this experiment has wall thickness of 3.5 mm, rendering the MNPs collection plane displaced further away from the magnet pole. Owing to this reason, the average magnetic field gradient imposed by NdFeB1 and NdFeB3 magnets on the MNPs collection plane are almost comparable, which are given by 68.4 T/m and 66.34 T/m respectively (Figures 10c & d). Secondly, NdFeB3 magnet creates larger MNPs collection plane A_s which attracts MNPs that are making physical contact with it. This can be observed in top view images displayed in Figure 10a as the immobilized MNPs layer on the bottom of the cuvette is larger when NdFeB3 magnet was employed. According to our calculation, $< A_s \frac{\partial B}{\partial z} >$ generated by NdFeB3 magnet on the MNPs solution in this magnetophoresis setup is given by 208.42 T m^{-1} cm^2, which is

relatively higher than that of NdFeB1 magnet (~105.26 T m^{-1} cm^2). This is the underlying reason which contributes to the faster magnetophoretic collection of MNPs induced by NdFeB3 magnet under this configuration. Again, results presented in this section are consistent with our hypothesized mechanism and mathematical model as the magnetophoretic rate of a fixed volume of MNPs solution increases with the magnitude of $< A_s \frac{\partial B}{\partial z} >$ imposed by the magnet on the MNPs collection plane.

The convective nature of low gradient magnetophoresis can be implemented in the separation of molecules or any targeted species by using MNPs with specific functionality as the influence of induced convection is able to extend to the remote region which is characterized by low magnetic field gradient. Owing to this unique property of magnetophoresis induced convection, the feature reported in this work can be utilized in the design of separation process conducted under different length scale ranging from microfluidic separation system to huge magnetic separator in the industry.

5. Conclusion

We have presented the mechanism of LGMS of superparamagnetic MNPs in which hydrodynamic interaction is dominating and convective flow is generated within the MNPs solution during magnetophoresis. This process requires highly inhomogeneous magnetic field gradients (such as those generated by a hand held permanent magnet), responsible for generating a mechanical instability (MNPs concentration gradient) in the fluid which subsequently leads to the convective flow. In accordance to this mechanism, a mathematical model was developed to depict LGMS process with the following assumptions: (1) MNPs solution is homogeneous throughout the entire timescale of magnetophoresis due to the agitation performed by the induced convection, (2) MNPs are continuously withdrawn from

the suspension and immobilized on the MNPs collection plane which is characterized by the strongest magnetic field gradient within the whole domain of MNPs solution. These hypothesis are supported by previous experimental observations and numerical results of hydrodynamic computer simulations. This model predicted that the batchwise LGMS process obeys first order kinetics, with an exponential decay of the concentration with time. This observation has been verified experimentally in our previous and current works and agreed with our proposed model excellently ($R^2 > 0.95$ for all cases).

The magnetophoretic separation rate is thus determined by the decay time constant τ, and the model predicts how the different physical properties affect this decay time. The model predicts that the time constant τ is directly proportional to the volume of MNPs solution subjected to magnetophoresis, which is in full agreement with experiments. In addition, according to the model the separation factor α (which is the reciprocal of the gradient of τ against solution volume V graph) is proportional to the product of the magnetic field gradient just on the collection plane and the total area of the collection plane, which is again in agreement with experimental results. As a consequence, we have found both theoretically and experimentally that the magnetic field distribution across the MNPs solution exerts no impact on the magnetophoretic collection rate of MNPs as long as induced convection exists and dominates the entire magnetophoresis process. This finding has important implications in the design and optimization of magnetic separator as it is no longer necessary to consider the spatial distribution of magnetic field across the whole domain of magnetic separator. In short, we only have to create the strongest magnetic field gradient on the MNPs collection plane in order to shorten the magnetic separation time of a magnetic separator!

Appendix

A1. Derivation of magnetophoretic force F_m exerted on a MNP suspended in solution

Generally, the magnetophoretic force $\overrightarrow{F_m}$ experienced by MNPs with magnetic dipole moment $\vec{m}$ under magnetic field $\vec{B}$ is given by the following equation:

$$\overrightarrow{F_m} = (\vec{m} \cdot \nabla)\vec{B} \tag{A1}$$

where ∇ is vector del operator which is expressed as:

$$\nabla = \frac{\partial}{\partial x}\overrightarrow{e_x} + \frac{\partial}{\partial y}\overrightarrow{e_y} + \frac{\partial}{\partial z}\overrightarrow{e_z} \tag{A2}$$

Here, $\overrightarrow{e_x}$, $\overrightarrow{e_y}$ and $\overrightarrow{e_z}$ are unit vectors pointing to x, y and z directions respectively.

Upon the exposure to an external magnetic field, MNPs acquire net magnetic dipole moment and align spontaneously such that the magnetic dipole moment is pointing toward the direction of local magnetic field strength $\vec{B}$. Therefore, the magnetic dipole moment vector $\vec{m}$ of MNP is always parallel to the magnetic field strength $\vec{B}$ at the position where it is located:

$$\vec{m} \parallel \vec{B} \tag{A3}$$

The magnitude of the magnetic dipole moment $|\vec{m}|$ is given by m:

$$|\vec{m}| = m \tag{A4}$$

According to these assumptions, Equation (A1) can be expressed as:

$$\overrightarrow{F_m} = \frac{|\vec{m}|}{B}(\vec{B} \cdot \nabla)\vec{B} = \frac{m}{B}(\vec{B} \cdot \nabla)\vec{B} \tag{A5}$$

where B is the magnitude of magnetic field strength. Yet, in accordance to chain rule in vector calculus,

$$\frac{1}{2}\nabla(\vec{A}\cdot\vec{A}) = (\vec{A}\cdot\nabla)\vec{A} + \vec{A}\times(\nabla\times\vec{A}) \quad \text{(A6)}$$

$(\vec{B}\cdot\nabla)\vec{B}$ term in Equation (A5) can be written as

$$(\vec{B}\cdot\nabla)\vec{B} = \frac{1}{2}\nabla(\vec{B}\cdot\vec{B}) - \vec{B}\times(\nabla\times\vec{B}) \quad \text{(A7)}$$

In magnetophoresis experiment, the curl of magnetic field $\nabla\times\vec{B}$ is zero as there is no time-varying electric field and flowing electric current inside the sample. Hence, Equation (A7) can be further simplified as:

$$(\vec{B}\cdot\nabla)\vec{B} = \frac{1}{2}\nabla(\vec{B}\cdot\vec{B}) \quad \text{(A8)}$$

By substituting Equation (A8) into Equation (A5),

$$\overrightarrow{F_m} = \frac{m}{2|\vec{B}|}\nabla(\vec{B}\cdot\vec{B}) = \frac{m}{2|\vec{B}|}\nabla B^2 = m\nabla B = m\frac{\partial B}{\partial x}\overrightarrow{e_x} + m\frac{\partial B}{\partial y}\overrightarrow{e_y} + m\frac{\partial B}{\partial z}\overrightarrow{e_z} \quad \text{(A9)}$$

According to Equation (A9), the absolute value of the z-component of magnetophoretic force $F_{m,z}$ is given by:

$$F_{m,z} = m\frac{\partial B}{\partial z} \quad \text{(A10)}$$

The magnetic dipole moment possessed by a MNP can be calculated from the product of volumetric magnetization M and volume of the given MNP:

$$m = \frac{\pi d^3 M}{6} \quad \text{(A11)}$$

where d is the diameter of the MNP. By inserting Equation (A11) into Equation (10),

$$F_{m,z} = \frac{\pi d^3 M}{6}\frac{\partial B}{\partial z} \quad \text{(A12)}$$

Equation (1) is resulted.

A2. Calculation of surface average of magnetic field gradient in z-direction $\langle\frac{\partial B}{\partial z}\rangle$ on MNPs collection plane

The following discussion describes the derivation of Equations (19) and (20) comprehensively. Figure A1a illustrates the top view of the magnetophoresis experimental setup (Figure 3). The blue region (it is the bottom of the cuvette and in square shape) is MNPs collection plane where MNPs are being magnetophoretically captured and immobilized. Here, we wish to calculate the surface average of magnetic field gradient $\langle\frac{\partial B}{\partial z}\rangle$ on the MNPs collection plane. Due to the cylindrical symmetry of the magnet employed, magnetic field gradient $\frac{\partial B}{\partial z}$ at a particular vertical displacement (or height) from the magnet pole is only the function of radial distance r from the cylindrical axis:

$$\frac{\partial B}{\partial z} = \frac{\partial B}{\partial z}(r) \tag{A13}$$

Apart from that, the area of infinitesimal surface element also can be expressed as the function of radial distance r (Figures A1b and A1c). Yet, according to the range of r, the expression for the area of infinitesimal surface element on the MNPs collection plane can be written in distinct form. For $r \leq R$, as illustrated in Figure A1b, the area of infinitesimal surface element (shaded region) can be expression as:

$$dA(r) = 2\pi r\, dr \tag{A14}$$

Here, $2\pi r$ is the circumference of the circle while dr is the thickness of the ring-shaped infinitesimal surface element. On the other hand, the the case of $r > R$, the infinitesimal surface element is no longer in the shape of complete ring (Figure A1c) and, hence, Equation

(A14) cannot be used to represent the area of the infinitesimal surface element. For simplicity, the following discussion demonstrates the derivation of $dA(r)$ for only one quadrant (as demonstrated in Figure A1d). By applying trigonometry function on one of the right-angled triangles in Figure A1d, the following expression can be written:

$$\cos\alpha = \frac{R}{r} \tag{A15}$$

Henceforth,

$$\alpha = \cos^{-1}\frac{R}{r} \tag{A16}$$

By subtracting 2α from a right angle (which is $\frac{\pi}{2}$ rad), θ can be written as:

$$\theta = \frac{\pi}{2} - 2\alpha = \frac{\pi}{2} - 2\cos^{-1}\frac{R}{r} \tag{A17}$$

Consequently, the arc length s (red colour) in Figure A1d can be formulated as:

$$s = r\theta = r\left(\frac{\pi}{2} - 2\cos^{-1}\frac{R}{r}\right) \tag{A18}$$

If the differential radial distance dr is sufficiently small, the area of the shaded region A can be expressed as:

$$A = s\,dr = r\left(\frac{\pi}{2} - 2\cos^{-1}\frac{R}{r}\right)dr \tag{A19}$$

Owing to its cylindrical symmetry, all quadrants in Figure A1c are characterized by the same mathematical formula. Therefore, the area of infinitesimal surface element (shaded region in Figure Alc) for the case of $r > R$ can be formulated as four times of Equation (A19):

$$dA(r) = 4A = 2r\left(\pi - 4\cos^{-1}\frac{R}{r}\right)dr \tag{A20}$$

However, for a square-shaped MNPs collection plane as illustrated in Figure A1a, the points characterized by the largest radial distance (furthest away from the center of the surface) are the vertices of the surface itself where the magnitude of the radial distance is given by $\sqrt{2}R$ (can be proven easily by using Pythagoras' Theorem). Therefore, Equation (A20) is only valid in the range of $R < r \leq \sqrt{2}R$. In short, the area of infinitesimal surface element $dA(r)$ on the MNPs collection plane can be written as the function of radial distance from the cylindrical axis r:

$$dA(r) = \begin{cases} 2\pi r\, dr, & 0 < r \leq R \\ 2r\left(\pi - 4\cos^{-1}\dfrac{R}{r}\right) dr, & R < r \leq \sqrt{2}R \end{cases} \quad \text{(A21)}$$

Finally, the surface average of magnetic field gradient $\langle\frac{\partial B}{\partial z}\rangle$ is expressed as:

$$\langle\frac{\partial B}{\partial z}\rangle = \frac{1}{A_s}\iint \frac{\partial B}{\partial z}\, dA \quad \text{(A22)}$$

Since, both the magnetic field gradient $\frac{\partial B}{\partial z}(r)$ and the area of infinitesimal surface element $dA(r)$ can be expressed as the function of radial distance r, the surface integral in Equation (A22) can be transformed into single integral (with only one variable r) as shown below:

$$\langle\frac{\partial B}{\partial z}\rangle = \frac{1}{A_s}\int_{r=0}^{r=\sqrt{2}R} \frac{\partial B}{\partial z}(r)\, dA(r) \quad \text{(A23)}$$

Nonetheless, there is no analytical solution for $\frac{\partial B}{\partial z}(r)$ and it only can be calculated by numerically solving Biot-Savart Law. The average magnetic field gradient $\langle\frac{\partial B}{\partial z}\rangle$ at MNPs collection plane with different elevations was computed by solving Equation (A23) numerically by the aid of MATLAB.

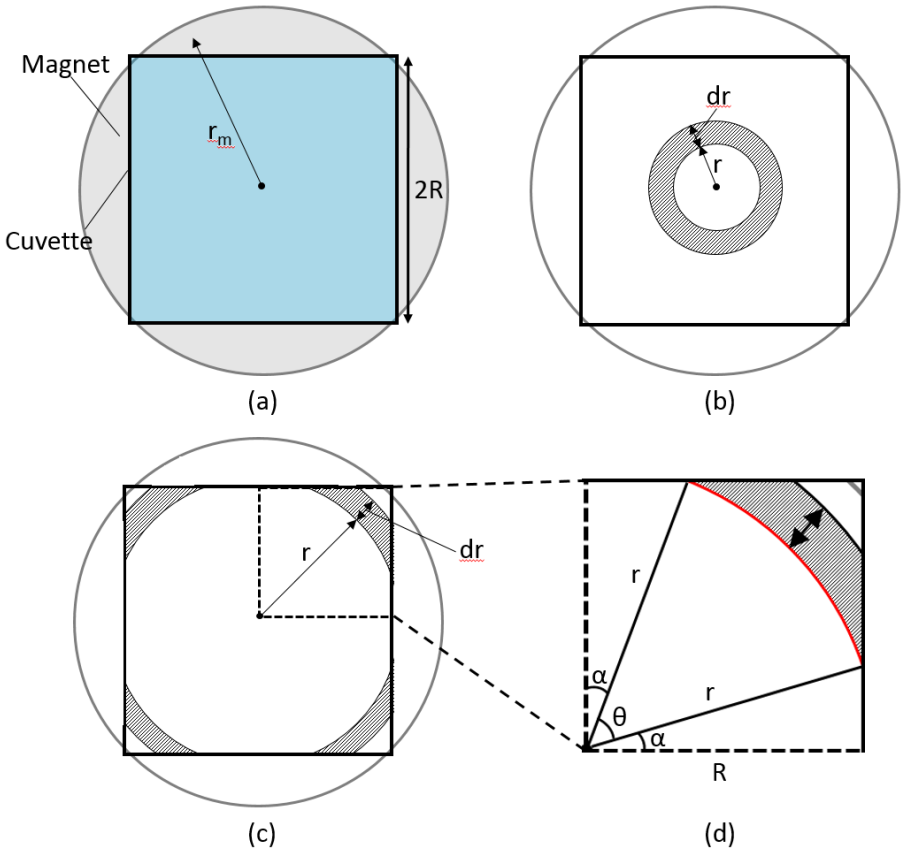

Figure A1. *(a) The top view of magnetophoresis setup in current study (Please refer to Figure 3 for 3-dimensional view). The blue square represents cuvette's bottom wall which is acting as MNPs collection plane. The grey circle is indicating the top view (or pole) of the cylindrical magnet used in magnetophoresis experiment. (b) The illustration for infinitesimal surface element for* $0 < r \leq R$. *(c) The illustration for infinitesimal surface element for* $R < r \leq \sqrt{2}R$. *(d) The zoom in image for a quadrant in (c). This figure serves as an illustration to the derivation of Equation (A21). The thickness of the surface element dr should be infinitesimal small in reality. The surface element shown has been enlarged for illustration purpose.*

A3. Calculation of average displacement between MNPs collection plane and magnet pole

As the cuvette bottom wall (which is acting as MNPs collection plane) is not a flat plane, it is essential to consider the geometrical effect of the collection plane throughout the data analysis. This issue is of particularly importance because the magnetic separation is greatly influenced by the magnetic field gradient on the collection plane, which in turn dictated by the elevation of the collection plane from the magnet pole.

The cuvette used in the experiments reported in current article is the standard disposable cuvette (DTS0012). The side view and top view of the cuvette bottom wall is illustrated in Figures A2a & A2b, in which the wall thickness and side length of the cuvette bottom wall are given by h_s cm and R cm, respectively. Also, there is a concave surface located at the center of the bottom wall, with a maximum elevation of h_{max} cm with respect to the flat surface and the projected radius of R_c cm. Furthermore, the thickness of the double-sided tape (which is holding the cuvette on the magnet throughout the entire timescale of experiment) is denoted as h_d cm. In order to predict the magnetic field gradient imposed on the MNPs collection plane, it is imperative to calculate the average elevation of the given surface (highlighted in red colour in Figure A2a) by taking the concave geometry into consideration.

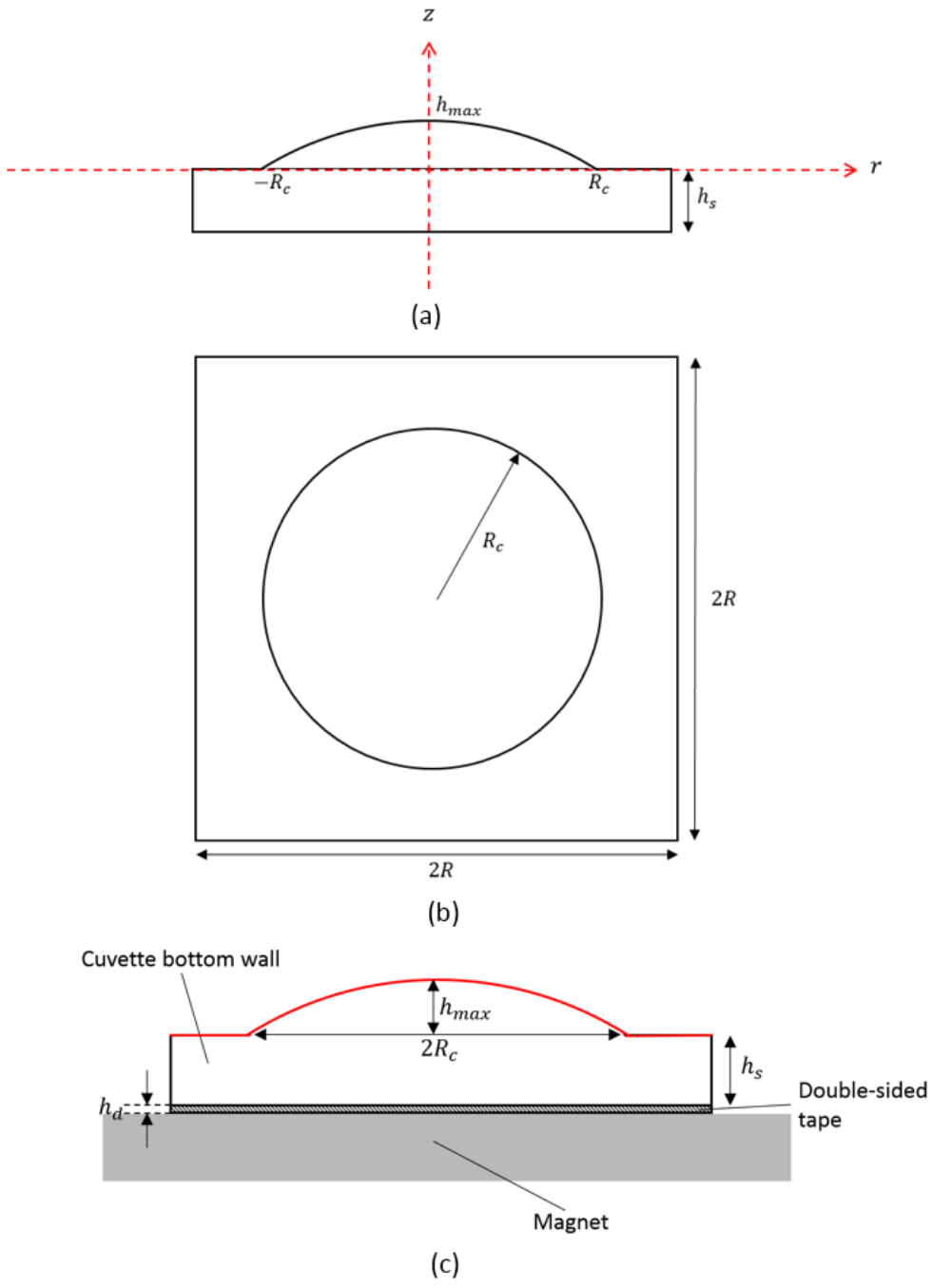

Figure A2. *(a) Side view of the cuvette bottom wall. (b) Top view of the cuvette bottom wall. (c) Illustration of axis assignation in computing the equation (Equation (1)) which represents the bolded curve.*

Here, the concave surface is approximated as a parabola and the cross sectional line of the surface (the bolded inverse U-shape curve in Figure A2c) can be fitted into a quadratic curve as shown below:

$$z = ar^2 + h_{max} \tag{A24}$$

where a is a constant. We assigned the elevation of the flat surface at the bottom wall is located at $z = 0$ for convenience of calculation. As $r = \pm R_c$, $z = 0$. Hence, after solving Equation (1) with this boundary condition, the constant a is evaluated as:

$$a = -\frac{h_{max}}{R_c^2} \tag{A25}$$

By substituting Equation (A25) back into Equation (A24), the following expressed is obtained:

$$z = h_{max}\left(1 - \frac{r^2}{R_c^2}\right) \tag{A26}$$

In order to calculate the average elevation of the concave surface $\langle z \rangle_c$ (with respect to the flat surface), the following surface integration is performed:

$$\langle z \rangle_c = \frac{\int_{\theta=0}^{\theta=2\pi}\int_{r=0}^{r=R_c} z\, r\, dr\, d\theta}{\pi R_c^2} = \frac{\int_{\theta=0}^{\theta=2\pi}\int_{r=0}^{r=R_c} h_{max}\left(1 - \frac{r^2}{R_c^2}\right) r\, dr\, d\theta}{\pi R_c^2} \tag{A27}$$

After performing the integration and simplification on Equation (A27), the average elevation of the concave surface $\langle z \rangle_c$ is resulted as follows:

$$\langle z \rangle_c = \frac{h_{max}}{2} \tag{A28}$$

Next, the average elevation of the whole MNPs collection plane $\langle z \rangle$ (with respect to the reference level $z = 0$) can be calculated by:

$$\langle z \rangle = \frac{\pi R_c^2 \left(\frac{h_{max}}{2}\right) + (4R^2 - \pi R_c^2)(0)}{4R^2} = \frac{\pi h_{max}}{8}\left(\frac{R_c}{R}\right)^2 \quad \text{(A29)}$$

Thus, the average thickness of the cuvette bottom surface h_t is given by:

$$h_t = \langle z \rangle + h_s = \frac{\pi h_{max}}{8}\left(\frac{R_c}{R}\right)^2 + h_s \quad \text{(A30)}$$

For the case without spacer being inserted between the cuvette and the magnet, the average elevation of cuvette bottom wall (or MNPs collection plane) from the magnet pole are given by:

$$\text{Average elevation} = \ h_t + h_d = \frac{\pi h_{max}}{8}\left(\frac{R_c}{R}\right)^2 + h_s + h_d \quad \text{(A31)}$$

According to our measurement by using Vernier caliper, R_c = 0.35 cm, R = 0.5 cm, h_{max} = 0.08 cm, h_s = 0.13 cm and h_d = 0.02 cm. By inserting these values into Equation (A31), the average elevation of the MNPs collection plane from the magnet pole (for the case without spacer inserted in between the magnet and the cuvette) is given by 0.165 cm (or 1.65 mm). Thus, in the curve fitting of the experimental data (Figure 8 in the main manuscript), we have to consider this elevation during the calculation of average magnetic field gradient $\langle \frac{\partial B}{\partial z} \rangle$ imposed on the MNPs collection plane.

Supporting Information available: (Section S1) Theoretical calculation of magnetophoretic separation time of 30 nm MNP and 200 nm MNP cluster, (Section S2) Justification for the negligible gravitational pull in our magnetophoresis system, (Section S3) Illustration of convection velocity and concentration profile from COMSOL hydrodynamic simulations, (Section S4) Justification of capture efficiency f = 1 of the particle system, (Section S5) Validity of Beer-Lambert's Law, (Section S6) The details of magnet employed in this study, (Section S7) Magnetic field gradient profile of magnets, (Section S8) Separation kinetic profiles and computation of separation factor α, (Section S9) Additional experimental data for Section 4.4.

Acknowledgement

SSL acknowledges the support from the Ministry of Higher Education of Malaysia through the MyPhD Scholarship. This project was also financially supported by FRGS grant from MOHE (Grant no. 203/PJKIMIA/6071269) and International Foundation for Science (IFS) which is co-financed by the Organization for the Prohibition of Chemical Weapon (OPCW) (Grant no. 304/PJKIMIA/6050324). JC and JF acknowledge Generalitat de Catalunya for Grant 2014 SGR 64. JF acknowledges financial support to ICMAB from the Spanish Ministry of Economy and Competitiveness, through the "Severo Ochoa" Programme for Centres of Excellence in R&D (SEV- 2015-0496). We acknowledge Asier Rabasco for help in some of the Figures in Supporting Information.

Abbreviations

HGMS, high gradient magnetic separation; LGMS, low gradient magnetic separation; MNPs, magnetic nanoparticles; PEG, polyethylene glycol; TEM, Transmission electron microscopy; DLS, dynamic light scattering; VSM, Vibrating sample magnetometer.

References

1. Surugau, N.; Urban, P. L. Electrophoretic Methods for Separation of Nanoparticles. *Journal of Separation Science* **2009**, *32*, 1889-1906.

2. Bhatt, K. H.; Velev, O. D. Control and Modeling of the Dielectrophoretic Assembly of On-Chip Nanoparticle Wires. *Langmuir* **2004**, *20*, 467-476.

3. Kawamata, T.; Yamada, M.; Yasuda, M.; Seki, M. Continuous and Precise Particle Separation by Electroosmotic Flow Control in Microfluidic Devices. *ELECTROPHORESIS* **2008**, *29*, 1423-1430.

4. Lim, J.; Lanni, C.; Evarts, E. R.; Lanni, F.; Tilton, R. D.; Majetich, S. A. Magnetophoresis of Nanoparticles. *ACS Nano* **2011**, *5*, 217-226.

5. Jauffred, L.; Taheri, S. M.-R.; Schmitt, R.; Linke, H.; Oddershede, L. B. Optical Trapping of Gold Nanoparticles in Air. *Nano Letters* **2015**, *15*, 4713-4719.

6. Tran, N.; Webster, T. J. Magnetic Nanoparticles: Biomedical Applications and Challenges. *Journal of Materials Chemistry* **2010**, *20*, 8760-8767.

7. Pankhurst, Q. A.; Connolly, J.; Jones, S. K.; Dobson, J. Applications of Magnetic Nanoparticles in Biomedicine. *Journal of Physics D: Applied Physics* **2003**, *36*, R167.

8. Catherine, C. B. Progress in Functionalization of Magnetic Nanoparticles for Applications in Biomedicine. *Journal of Physics D: Applied Physics* **2009**, *42*, 224003.

9. De Jong, W. H.; Borm, P. J. A. Drug Delivery and Nanoparticles: Applications and Hazards. *International Journal of Nanomedicine* **2008**, *3*, 133-149.

10. Lee, J.-H.; Kim, J.-w.; Cheon, J. Magnetic Nanoparticles for Multi-Imaging and Drug Delivery. *Molecules and Cells* **2013**, *35*, 274-284.

11. Andreu, J. S.; Camacho, J.; Faraudo, J. Aggregation of Superparamagnetic Colloids in Magnetic Fields: the Quest for the Equilibrium State. *Soft Matter* **2011**, *7*, 2336-2339.

12. Yellen, B. B.; Hovorka, O.; Friedman, G. Arranging Matter by Magnetic Nanoparticle Assemblers. *Proceedings of the National Academy of Sciences of the United States of America* **2005**, *102*, 8860-8864.

13. Erb, R. M.; Son, H. S.; Samanta, B.; Rotello, V. M.; Yellen, B. B. Magnetic Assembly of Colloidal Superstructures with Multipole Symmetry. *Nature* **2009**, *457*, 999-1002.

14. Mayo, J. T.; Lee, S. S.; Yavuz, C. T.; Yu, W. W.; Prakash, A.; Falkner, J. C.; Colvin, V. L. A Multiplexed Separation of Iron Oxide Nanocrystals using Variable Magnetic Fields. *Nanoscale* **2011**, *3*, 4560-4563.

15. Yavuz, C. T.; Prakash, A.; Mayo, J. T.; Colvin, V. L. Magnetic Separations: From Steel Plants to Biotechnology. *Chemical Engineering Science* **2009**, *64*, 2510-2521.

16. Chen, Y.; Xianyu, Y.; Wang, Y.; Zhang, X.; Cha, R.; Sun, J.; Jiang, X. One-Step Detection of Pathogens and Viruses: Combining Magnetic Relaxation Switching and Magnetic Separation. *ACS Nano* **2015**, *9*, 3184-3191.

17. Pamme, N.; Wilhelm, C. Continuous Sorting of Magnetic Cells via On-Chip Free-Flow Magnetophoresis. *Lab on a Chip* **2006**, *6*, 974-980.

18. De Palma, R.; Liu, C.; Barbagini, F.; Reekmans, G.; Bonroy, K.; Laureyn, W.; Borghs, G.; Maes, G. Magnetic Particles as Labels in Bioassays: Interactions between a Biotinylated Gold Substrate and Streptavidin Magnetic Particles. *The Journal of Physical Chemistry C* **2007**, *111*, 12227-12235.

19. Song, E.-Q.; Hu, J.; Wen, C.-Y.; Tian, Z.-Q.; Yu, X.; Zhang, Z.-L.; Shi, Y.-B.; Pang, D.-W. Fluorescent-Magnetic-Biotargeting Multifunctional Nanobioprobes for Detecting and Isolating Multiple Types of Tumor Cells. *ACS Nano* **2011**, *5*, 761-770.

20. Zborowski, M.; Chalmers, J. J.; Webster, J. G. Magnetophoresis: Fundamentals and Applications. In *Wiley Encyclopedia of Electrical and Electronics Engineering*, John Wiley & Sons, Inc.: **1999**.

21. Oberteuffer, J. Magnetic Separation: A Review of Principles, Devices, and Applications. *IEEE Transactions on Magnetics* **1974**, *10*, 223-238.

22. Moeser, G. D.; Roach, K. A.; Green, W. H.; Alan Hatton, T.; Laibinis, P. E. High-Gradient Magnetic Separation of Coated Magnetic Nanoparticles. *AIChE Journal* **2004**, *50*, 2835-2848.

23. Corchero, J. L.; Villaverde, A. Biomedical Applications of Distally Controlled Magnetic Nanoparticles. *Trends in Biotechnology* **2009**, *27*, 468-476.

24. Gómez-Pastora, J.; Bringas, E.; Ortiz, I. Recent Progress and Future Challenges on the Use of High Performance Magnetic Nano-Adsorbents in Environmental Applications. *Chemical Engineering Journal* **2014**, *256*, 187-204.

25. Mariani, G.; Fabbri, M.; Negrini, F.; Ribani, P. L. High-Gradient Magnetic Separation of Pollutant from Wastewaters using Permanent Magnets. *Separation and Purification Technology* **2010**, *72*, 147-155.

26. Saha, B.; Das, S.; Saikia, J.; Das, G. Preferential and Enhanced Adsorption of Different Dyes on Iron Oxide Nanoparticles: A Comparative Study. *The Journal of Physical Chemistry C* **2011**, *115*, 8024-8033.

27. Liu, M.; Chen, C.; Hu, J.; Wu, X.; Wang, X. Synthesis of Magnetite/Graphene Oxide Composite and Application for Cobalt(II) Removal. *The Journal of Physical Chemistry C* **2011**, *115*, 25234-25240.

28. Shao, D.; Hu, J.; Chen, C.; Sheng, G.; Ren, X.; Wang, X. Polyaniline Multiwalled Carbon Nanotube Magnetic Composite Prepared by Plasma-Induced Graft Technique and Its Application for Removal of Aniline and Phenol. *The Journal of Physical Chemistry C* **2010**, *114*, 21524-21530.

29. Prochazkova, G.; Safarik, I.; Branyik, T. Harvesting Microalgae with Microwave Synthesized Magnetic Microparticles. *Bioresource Technology* **2013**, *130*, 472-477.

30. Yavuz, C. T.; Mayo, J. T.; Yu, W. W.; Prakash, A.; Falkner, J. C.; Yean, S.; Cong, L.; Shipley, H. J.; Kan, A.; Tomson, M.; Natelson, D.; Colvin, V. L. Low-Field Magnetic Separation of Monodisperse Fe3O4 Nanocrystals. *Science* **2006**, *314*, 964-967.

31. De Las Cuevas, G.; Faraudo, J.; Camacho, J. Low-Gradient Magnetophoresis through Field-Induced Reversible Aggregation. *The Journal of Physical Chemistry C* **2008**, *112*, 945-950.

32. Faraudo, J.; Camacho, J. Cooperative Magnetophoresis of Superparamagnetic Colloids: Theoretical Aspects. *Colloid and Polymer Science* **2010**, *288*, 207-215.

33. Lim, J.; Yeap, S. P.; Low, S. C. Challenges Associated to Magnetic Separation of Nanomaterials at Low Field Gradient. *Separation and Purification Technology* **2014**, *123*, 171-174.

34. Leong, S. S.; Ahmad, Z.; Lim, J. Magnetophoresis of Superparamagnetic Nanoparticles at Low Field Gradient: Hydrodynamic Effect. *Soft Matter* **2015**, *11*, 6968-6980.

35. Schaller, V.; Kräling, U.; Rusu, C.; Petersson, K.; Wipenmyr, J.; Krozer, A.; Wahnström, G.; Sanz-Velasco, A.; Enoksson, P.; Johansson, C. Motion of Nanometer Sized Magnetic Particles in a Magnetic Field Gradient. *Journal of Applied Physics* **2008**, *104*, 093918.

36. Faraudo, J.; Andreu, J. S.; Camacho, J. Understanding Diluted Dispersions of Superparamagnetic Particles under Strong Magnetic Fields: A Review of Concepts, Theory and Simulations. *Soft Matter* **2013**, *9*, 6654-6664.

37. Faraudo, J.; Andreu, J. S.; Calero, C.; Camacho, J. Predicting the Self-Assembly of Superparamagnetic Colloids under Magnetic Fields. *Advanced Functional Materials* **2016**, *26*, 3837-3858.

38. Zhao, Z.; Torres-Díaz, I.; Vélez, C.; Arnold, D.; Rinaldi, C. Brownian Dynamics Simulations of Magnetic Nanoparticles Captured in Strong Magnetic Field Gradients. *The Journal of Physical Chemistry C* **2017**, *121(1)*, 801-810.

39. Xue, X.; Furlani, E. P. Analysis of the Dynamics of Magnetic Core–Shell Nanoparticles and Self-Assembly of Crystalline Superstructures in Gradient Fields. *The Journal of Physical Chemistry C* **2015**, *119*, 5714-5726.

40. Andreu, J. S.; Calero, C.; Camacho, J.; Faraudo, J. On-the-Fly Coarse-Graining Methodology for the Simulation of Chain Formation of Superparamagnetic Colloids in Strong Magnetic Fields. *Physical Review E* **2012**, *85*, 036709.

41. Andreu, J. S.; Camacho, J.; Faraudo, J.; Benelmekki, M.; Rebollo, C.; Martínez, L. M. Simple Analytical Model for the Magnetophoretic Separation of Superparamagnetic Dispersions in a Uniform Magnetic Gradient. *Physical Review E* **2011**, *84*, 021402.

42. Andreu, J. S.; Barbero, P.; Camacho, J.; Faraudo, J. Simulation of Magnetophoretic Separation Processes in Dispersions of Superparamagnetic Nanoparticles in the Noncooperative Regime. *Journal of Nanomaterials* **2012**, *2012*, 10.

43. Xia, N.; Hunt, T. P.; Mayers, B. T.; Alsberg, E.; Whitesides, G. M.; Westervelt, R. M.; Ingber, D. E. Combined Microfluidic-Micromagnetic Separation of Living Cells in Continuous Flow. *Biomedical Microdevices* **2006**, *8*, 299.

44. Furlani, E. P. Analysis of Particle Transport in a Magnetophoretic Microsystem. *Journal of Applied Physics* **2006**, *99*, 024912.

45. Furlani, E. P.; Sahoo, Y. Analytical Model for the Magnetic Field and Force in a Magnetophoretic Microsystem. *Journal of Physics D: Applied Physics* **2006**, *39*, 1724.

46. Furlani, E. P.; Sahoo, Y.; Ng, K. C.; Wortman, J. C.; Monk, T. E. A Model for Predicting Magnetic Particle Capture in a Microfluidic Bioseparator. *Biomedical Microdevices* **2007**, *9*, 451-463.

47. Benelmekki, M.; Martinez, L. M.; Andreu, J. S.; Camacho, J.; Faraudo, J. Magnetophoresis of Colloidal Particles in a Dispersion of Superparamagnetic Nanoparticles: Theory and Experiments. *Soft Matter* **2012**, *8*, 6039-6047.

48. Kucheryavy, P.; He, J.; John, V. T.; Maharjan, P.; Spinu, L.; Goloverda, G. Z.; Kolesnichenko, V. L. Superparamagnetic Iron Oxide Nanoparticles with Variable Size and an Iron Oxidation State as Prospective Imaging Agents. *Langmuir* **2013**, *29*, 710-716.

49. Callister, W. D.; Rethwisch, D. G. *Materials Science and Engineering: An Introduction, 8th Edition*. Wiley: **2009**.

50. Lim, J.; Yeap, S. P.; Leow, C. H.; Toh, P. Y.; Low, S. C. Magnetophoresis of Iron Oxide Nanoparticles at Low Field Gradient: The Role of Shape Anisotropy. *Journal of Colloid and Interface Science* **2014**, *421*, 170-177.

51. Yeap, S. P.; Leong, S. S.; Ahmad, A. L.; Ooi, B. S.; Lim, J. On Size Fractionation of Iron Oxide Nanoclusters by Low Magnetic Field Gradient. *The Journal of Physical Chemistry C* **2014**, *118*, 24042-24054.

52. Bird, R. B.; Stewart, W. E.; Lightfoot, E. N. *Transport Phenomena*. 2nd edition ed.; John Wiley & Sons, Inc.: **2006**.

53. Berne, B. J.; Pecora, R. *Dynamic Light Scattering: With Applications to Chemistry, Biology, and Physics*. Dover Publications: **2013**.

54. Ocean NanoTech, Iron Oxide Nanoparticles with PEG. https://www.oceannanotech.com/upload/120615172122737283kzixtw.pdf

TOC Image

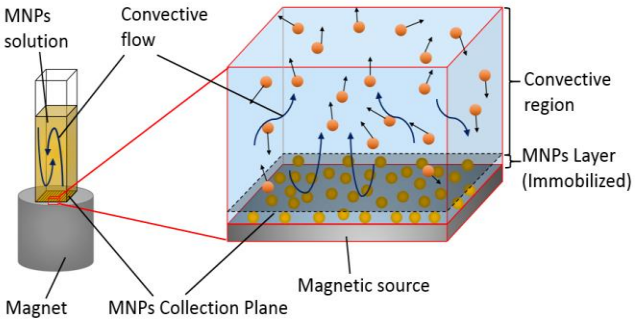
MNPs solution
Convective flow
Convective region
MNPs Layer (Immobilized)
Magnetic source
Magnet
MNPs Collection Plane